Unintended Consequences of Environmental Regulation of Maritime Shipping: Carbon Leakage to Air Shipping*

Volodymyr Lugovskyy† Alexandre Skiba‡ David Terner§

This draft: October 2024
First draft: October 2022

Abstract

We assess the expected impact of the upcoming International Maritime Organization's CO_2 emissions cap on global maritime shipping. Using detailed data on U.S. imports—covering vessels, routes, emissions, and trade—we estimate a model that allows for substitution between maritime, air, and land transport. Our findings show that the cap will drive a shift to more carbon-intensive air and land transport, leading to an overall increase in transportation-related CO_2 emissions in both the short- and long-run. Additionally, it will cause significant welfare losses. Our findings support a case for more efficient alternative policy options.

*We are grateful for the excellent feedback provided by Tibor Besedeš, Bruce Blonigen, Anca Cristea, Phillip Economides, Jan Hoffmann, David Hummels, Sam Kortum, Ahmad Lashkaripor, Mogens L. Mathiesen, Joseph Shapiro, Woan Foong Wong, Joshua Graff Zivin, and the participants at (the): University of Oregon Economics Seminar (Fall 2022); Midwest Macroeconomics Meetings (Fall 2022); Empirical Investigations in International Trade (Fall 2022); Midwest Economic Theory and International Trade Conference (Fall 2022); NERA Economic Consulting (Fall 2022); Indiana University Microeconomics Workshop (Fall 2022); Midwest Economic Theory and International Trade Conference (Spring 2022); Indiana University Trade Seminar (Spring 2022); and, Southern Economics Association Meetings (Fall 2021). We thank BlueWater Reporting for providing access to their data on maritime containerized ocean routes and carrier composition. All mistakes are our own.

†Department of Economics, Indiana University, Wylie Hall Rm 301, 100 S. Woodlawn, Bloomington, IN 47405; e-mail: vlugovsk@iu.edu

‡Department of Economics, University of Wyoming; 1000 E. University Ave, Laramie, WY 82071; e-mail: askiba@uwyo.edu

§NERA Economic Consulting; 360 Hamilton Ave, White Plains, NY 10601; e-mail: david.terner@nera.com

1 Introduction

The United Nations (U.N.) has identified global decarbonization as a top priority (Guterres, 2020). In line with this agenda, the U.N. mandated its International Maritime Organization (IMO) to spearhead the decarbonization of maritime transport, which handles 90% of international trade by weight (IMO, 2014). In response, the IMO adopted Initial IMO Strategy on Reduction of GHG Emissions, aimed at limiting CO_2 emissions from maritime transport. Originally scheduled for implementation in 2023, the timeline has been postponed, with Resolution MEPC.377(80) now setting the new implementation date for 2027 (IMO, 2023). We refer to these forthcoming regulations as IMO2023.

Our paper provides an ex-ante analysis of the potential impacts of the forthcoming IMO2023 regulations. Ocean transportation is the most CO_2-efficient mode of transport: per ton-mile, it emits 2.4 times less CO_2 than rail, 12.5 times less than road, and 103.5 times less than air transport (Shapiro, 2016). Therefore, while over 90% of global weight-miles are transported by sea, maritime shipping contributes just 3% of total global emissions—out of the 8% attributed to all cargo transport.[1]

Our central argument is that, while IMO2023 is intended to reduce emissions, it may have the unintended consequence of backfiring. By diverting freight from maritime shipping to far more carbon-intensive air and ground transportation, IMO2023 risks not only undermining environmental objectives but also driving up consumer costs, thereby diminishing overall welfare. Furthermore, if implemented, this reform could erode public trust in future environmental initiatives—potentially setting back broader efforts to combat climate change.

To quantitatively analyze the effects of IMO2023, we focus on U.S. imports of manufactured goods due to the absence of detailed global transportation cost data. By focusing on the U.S.—the world's largest importer—we can access the most detailed data available on freight rates, weights, and import prices, providing the foundation for rigorous empirical analysis. This focus also aligns with previous research that has specifically examined the interchangeability between air and maritime transport in

[1] See U.S. EPA, which indicates that in 2019, transportation contributed 15% of global CO_2 emissions, with more than half coming from goods transportation. Overall, transportation is the fourth-largest global emitter (after energy, industry, and AFOLU (Agriculture, Forestry, and Other Land Use), making it a crucial sector for any emissions-related discussion.

the context of U.S. imports (Harrigan, 2010; Hummels and Schaur, 2010, 2013), ensuring consistency and comparability with established findings.

As a starting point for our analysis, we compare IMO2023 emissions thresholds with actual vessel data and find that many exceed the limits. Expert opinions and official reports suggest that current abatement technologies are either insufficient or too costly to meet the new standards. As a result, both IMO members and shipping industry experts agree that, in the short term, slow-steaming—reducing vessel speeds—is the only viable strategy. Using vessel emissions data and naval engineering formulas, we calculate that U.S.-bound container vessels will need to reduce speeds by an average of 5.2%. Moreover, we show that slow-steaming will effectively reduce capacity in this already capacity-constrained industry. Specifically, we calculate that the reduction in capacity will vary significantly across U.S.-inbound routes, with an average decrease of about 5.2%—a figure consistent with industry expert estimates.

Next, to estimate critical parameters for evaluating IMO2023, we develop a model of U.S. imports at the Customs District level that accounts for substitution both between transportation modes and across routes. The model captures essential structural parameters, including the elasticities of substitution (i) within transportation modes on a given route and (ii) between different routes, as well as preference parameters for goods transported by various modes. We estimate these parameters using U.S. Census Imports data, combined with TransBorder Freight Data, which provide detailed information on transportation mode, freight rates, and quantities of U.S. imports at a highly disaggregated level.

Estimated demand- and supply-side parameters enable us to predict both the short-run and long-run impacts of IMO2023. By applying these parameters to our model's short-run predictions, we show that, for the U.S.-bound containerized ocean fleet, IMO2023 will (i) more than double the average freight rate and (ii) decrease CO_2 emissions by 15.6%. That is, IMO2023 will indeed achieve its targeted reduction in CO_2 emissions from ocean transportation. However, it will concurrently lead to a significant pollution leakage into air transportation: our model predicts an increase in CO_2 emissions related to air transportation by up to 12.4%. Consequently, combined CO_2 emissions from

both ocean and air transport will increase by up to 3.3%. This implies that in the short-run, the unintended consequences of IMO2023 will effectively negate its intended benefits, leading to an overall *increase* in total emissions.

Furthermore, the implications of IMO2023 extend beyond environmental consequences. The reform will also impact the economic dynamics of U.S. imports. Imported goods will be delivered at slower speeds, arrive in reduced quantities, and at much higher freight rates. These factors collectively contribute to significant welfare losses for American consumers, which we estimate to 45.8 billion USD annually. IMO members are the only player in this policy proposal that stands to accrue material benefits: the reform will enhance industry's image by reducing emissions produced by ocean transportation, increase short-run profits of carriers, and boost demand for new vessels in the medium and long-run. In our counterfactual analysis, we show that an effective, though unexpected, short-term policy would be to increase the speed of containerized vessels. This would raise total emissions by just 0.2% but boost consumer surplus by $3.8 billion.

Our long-term analysis shows that, while the effects of the IMO2023 reform are less dramatic, both the "green paradox" and significant welfare losses persist. We estimate a 2% annual increase in net emissions from transportation, coupled with $14 billion in yearly welfare losses. These outcomes indicate that the reform not only fails to address the emissions problem but may actually worsen it, imposing substantial economic costs without delivering meaningful environmental benefits.

In contrast, our long-run counterfactual analysis suggests that taxing air-transported goods could offer a more effective solution. By shifting demand toward more carbon-efficient ocean transport, this policy could lower overall pollution and reduce the welfare losses per percentage reduction in emissions.

A broader issue lies in the potential conflict of interest within self-regulating organizations like the IMO. With its members drawn from carriers, shipbuilders, and financiers, the IMO is likely to prioritize industry interests over global environmental goals, as suggested by Apuzzo and Hurtes (2021). This raises concerns about the organization's ability to enact policies that truly serve the public interest. Restructuring U.N. specialized agencies, though complex, could help ensure envi-

ronmental priorities take precedence over industry-driven policies, improving the U.N.'s ability to meet climate targets.

While we lack equivalent data for other countries, we find that the U.S. is not unique in its share of air-transported goods. Thus, we expect similar qualitative effects from IMO2023 for imports in other countries, leading to significant leakage into air transportation globally.

Our paper contributes to several bodies of literature. First, we contribute to the literature on government regulation of pollution and pollution leakages. In general, government intervention is a textbook solution for dealing with externalities, including environmental externalities (Pigou, 1920). Such intervention compels producers to internalize the external cost of pollution, thereby mitigating the impacts of market failure. However, the effects of regulation become ambiguous if controlling one market leads to increased pollution in another, a phenomenon known as leakage.

Pollution leakage has been thoroughly examined within the context of geographic markets, where regulation in one country or U.S. county increases pollution in others (e.g., Becker and Henderson, 2000; Greenstone, 2002).[2] We contribute to this literature by highlighting a different type of pollution leakage: inter-sectoral leakage from ocean to air transportation, where stricter regulations exclusively on ocean transportation will shift import demand from ocean to air transportation.

This unintended consequence of IMO2023 will be especially severe given that air transportation is two orders of magnitude more carbon-intensive than containerized maritime transportation.[3] This stark difference in carbon-intensity between the targeted ocean transportation and the leakage destination (air transportation) is unprecedented. Therefore, inter-modal leakage may not just undermine the effect of regulation, as in case of some other within-industry leakages,[4] but can even overturn it,

[2] There is a large body of literature on trade and environmental regulations, which focuses on the environmental aspects of trade, including international leakage and free riding across countries. A very incomplete list of papers in this literature includes Markusen (1975); Copeland (1996); Elliott et al. (2010); Hanna (2010); Nordhaus (2015); Shapiro (2020); Farrokhi and Lashkaripour (2021); Kortum and Weisbach (2021); Tanaka et al. (2022).

[3] According to our calculations, the average ratio of grams of CO_2 per ton of goods transported by air relative to American container ship routes results in a 90-fold difference. This 90-fold difference grows to 156 if we compare grams of CO_2 per ton-mile since air routes are typically more direct than container ship routes. Cristea et al. (2013) and Shapiro (2016) have also highlighted the much greater carbon intensity of air transportation compared to ocean and other modes of transportation.

[4] See, for example, literature on *Gruenspecht effect*, where the impact of stricter emission regulations of new vehicles is offset by the owners keeping older vehicles for longer time (Gruenspecht, 1982; Jacobsen and van Benthem, 2015).

increasing the overall emissions and creating a version of the *green paradox*.[5] While our study is limited to the maritime transportation sector, which contributes about 3% of the global CO_2 emissions and thus is unlikely to have major macroeconomic implications, the fact that the proposed reform is both costly and counterproductive is important and might provide useful insights for environmental regulation in other sectors.

Second, our paper contributes to academic research on emissions from transportation. Most research on pollution from transportation does not focus on the issue of leakage. Walker et al. (2019) offers a comprehensive review of the environmental effects of maritime transportation, Ben-Hakoun et al. (2016) focuses on carbon pollution by maritime transport, and Chao (2014) studies the cost-effect of carbon pollution caused by air cargo transportation. Recent work by Wong and Fuchs (2022) analyzes the impacts of improving inter-modal transport infrastructure, including container ports, on both welfare and mode-specific greenhouse emissions. Even research on spatial leakage of carbon emissions produced by maritime transport tends to ignore intersectoral leakage. Unsurprisingly, this research advocates for either quantitative emissions restrictions or taxes on bunker fuel in ocean transportation (Parry et al., 2018; Mundaca et al., 2021). According to our results, such policies are likely to *increase* joint air and ocean transportation emissions.

Our paper proceeds as follows. Section 2 provides an overview of IMO2023, our shipping microdata, and IMO2023 impacts on vessel speed and attendant short-run U.S. ocean-transportation capacity removal. Section 3 presents our theoretical model. We estimate and calibrate model parameters in Section 4. Section 5 presents short-run predictions on the effects of IMO2023, while Section 6 addresses long-run impacts and compares them against an alternative policy of taxing air-transported goods while leaving shipping speeds unchanged. Section 7 concludes and discusses the external validity of our findings to other countries.

[5] See der Werf and Maria (2012) for a review of green paradox literature related to pollution leakage.

2 The Anatomy of IMO2023

IMO2023 regulations, established by the International Maritime Organization (IMO), represent a critical step in the global effort to reduce carbon emissions from maritime transport, a significant contributor to global CO_2 emissions. As a specialized agency of the United Nations, the IMO has been tasked with developing global safety and environmental standards for the shipping industry. In 2018, the IMO introduced its Initial IMO Strategy on Reduction of GHG Emissions, which aims to progressively tighten carbon intensity standards for ships, measured as CO_2 emissions per ton-mile of cargo, with the goal of full implementation by 2050. Collectively known as IMO2023, these regulations mandate that ships meet increasingly strict Carbon Intensity Indicator (CII) targets.[6] Originally slated for 2023, IMO2023 regulations have encountered a significant delay. In July 2023, the Marine Environment Protection Committee (MEPC) convened for its 80th session, where it adopted Resolution MEPC.377(80). This resolution, formally known as the "2023 IMO Strategy on Reduction of GHG Emissions from Ships," now defers the enforcement of IMO2023 measures to 2027. While the timeline has shifted, the technical regulations outlined in earlier resolutions, including MEPC.304(72) and MEPC.328(76), remain intact. The only substantial change is the extended timeline for implementation. Consequently, the analysis presented in this paper retains its relevance as the industry prepares for the forthcoming reforms IMO (2023).

In this section, we dissect the legal underpinnings of IMO2023 and integrate them with naval engineering formulas to forecast the regulations' impact on vessel speed and fleet capacity. To support our analysis, we incorporate a range of relevant datasets. For ease of reference, these datasets are summarized in Table 1.

As noted earlier, IMO2023 imposes increasingly stringent Carbon Intensity Indicator (CII) targets on ships. These standards quantify CO_2 emissions in grams per ton-mile. For any given year t, a

[6] The origins of emission threshold policies can be traced back to the Initial IMO Strategy on Reduction of GHG Emissions adopted in April 2018 (IMO Resolution MEPC.304(72)), which was later expanded with new regulations approved in 2021 (refer to IMO Resolutions MEPC.335(76), MEPC.336(76), MEPC.337(76), MEPC.338(76)). On the enforcement side, failure to comply could result in operational restrictions, including being barred from certain ports or being unchartered.

Table 1: Summary of Datasets Used in Section 2

Name of the Dataset	Key Variables	Purpose of Using the Dataset	Section
IMO2023 Regulations	Required emissions per vessel size (Dead Weight Tonnage, Dwt)	To compare actual emissions per vessel with those required by IMO2023 regulations	2
World Fleet Register (WFR), Clarksons PLC	Dead Weight Tonnage (Dwt) and other technical characteristics of individual containerized vessels	To analyze current emissions by vessel size and calculate the required speed adjustments to meet IMO2023 standards	2
THETIS-MRV, by the European Maritime Safety Agency (EMSA)	Measured annual carbon emissions and distance traveled per vessel	To obtain actual per-vessel emissions data for comparison with the benchmark emissions set by IMO2023	2
Shipping Intelligence Network (SIN), Clarksons PLC	Idle capacity data for vessels	To demonstrate that containerized shipping operates at full capacity	2.2
Automatic Identification System (AIS), Marine Cadastre	AIS tracking data for container ships serving U.S. ports	To estimate port time and analyze its relationship with traffic levels	2.2

vessel's operational carbon efficiency, represented as $CIIv,t^{obs}$, is measured against the IMO's required CII, $CII^{req}v,t$. The formulas for these calculations are detailed in Table 2. The required CII is anchored to a reference level of CO_2 emissions, which is determined by a ship's deadweight tonnage (Dwt). A lower CII indicates greater carbon efficiency. The IMO assigns letter grades to ships based on the ratio $\frac{CIIv,t^{obs}}{CII^{req}v,t}$, with the grading thresholds specified in Table 2.

Table 2: IMO2023 Letter Grade Classification of Carbon Efficiency

$\frac{CII^{obs}_{v,t}}{CII^{req}_{v,t}} \times 100\%$	$< 83\%$	$83 - 94\%$	$94 - 107\%$	$107 - 119\%$	$> 119\%$
Grade	A	B	C	D	E

Note: $CII^{obs}_{v,t} = \frac{\text{CO}_2 \text{ Emissions}_{v,t}}{Dwt_v \times Dist_{v,t}}$ and $CII^{req}_{v,t} = \left[1984 \times (Dwt_v)^{-0.489}\right](1 - Z_t)$, where Dwt_v—Deadweight Tonnage— is a measure of vessel size; $Dist_{v,t}$ is the total distance traveled by v in year t; expression in $[.]$ is the reference line in year 2019; and Z_t was supposed to start out at 5% in 2023 and increments by 2% each year with the rate likely to accelerate in 2027 (Table 1 of MEPC.338(76)) As the implementation of IMO2023 has been postponed, the projected start date has been revised to 2027.

Starting in 2027—four years later than originally planned—only vessels earning an "A," "B," or "C" grade will be eligible for charter without significant operational modifications. Under the post-IMO2023 framework, the required Carbon Intensity Indicator ($CII^{req}_{v,t}$) will tighten each year, raising the bar for carbon efficiency. As a result, a vessel that earns a "C" grade in 2027 could easily find itself slipping to a failing "D" grade by 2028 if no adjustments are made to improve its performance.[7]

To assign letter grades to vessels based on IMO2023 standards, we leverage a meticulously con-

[7] See MEPC.354(78) for letter grades.

structed database of containerized vessels. This database includes the key metrics needed to calculate a vessel's observed carbon efficiency: deadweight tonnage (Dwt), distance traveled, and CO_2 emissions. We draw from three distinct data sources to capture these variables. First, Dwt data for all containerized vessels is sourced from the World Fleet Register (WFR), maintained by Clarksons PLC, the world's leading shipbroker. Second, we use BlueWater Reporting data to track port-to-port rotations and measure the annual distance traveled by each containership. Third, we rely on a partial dataset from THETIS-MRV (also known as THETIS), an online database managed by the European Maritime Safety Agency (EMSA), which provides information on carbon emissions and distance traveled for the years 2018-2023. This dataset covers 39.7% of the global containerized ocean fleet by count and 54.1% by capacity. Additional details on these and other datasets used in the paper can be found in Online Appendix A.1.

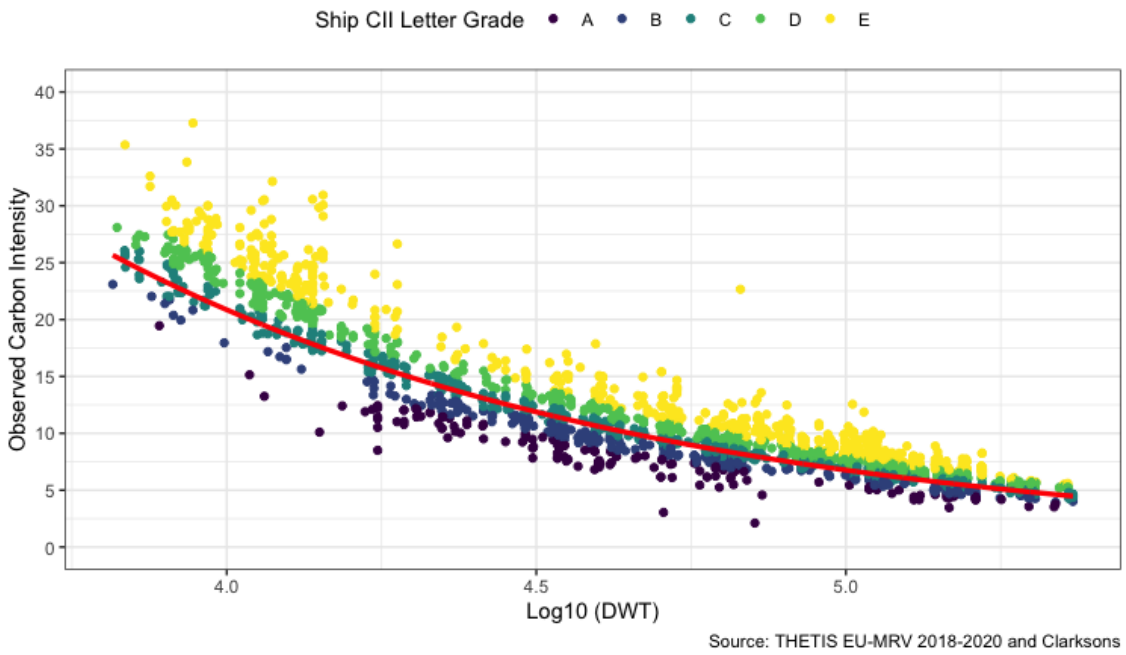


Figure 1: Observed Carbon Intensity
Notes: Each dot represents a vessel. Based on Dwt capacity, our sample has the following distribution of CII letter grades going based on IMO2023 required CII: 5.1% are A, 12.8% are B; 25.0% are C; 27.3% are D; and, 29.8% are E.

Using our vessel database, we perform two key analyses. First, we calculate IMO2023 letter grades for 1,903 containerized vessels included in the THETIS dataset, with the results displayed in

Figure 1. For vessels with multiple observations, we average the data at the vessel level to derive $\overline{CII}_v^{obs}$. Second, we estimate CO_2 emissions for the remaining vessels in the database to determine their corresponding letter grades. Using our vessel database, we conduct two key analyses. First, we calculate the average (across year) IMO2023 CII, $\overline{CII}_v^{obs}$, for 1,903 containerized vessels reported in the THETIS dataset, $\overline{CII}_v^{obs}$, and use vessels' CIIS to determine their letter grades. Second, we estimate CO_2 emissions for the remaining vessels to calculate their letter grades. Figure 1 displays the IMO2023 required CII benchmark efficiency line for 2027 (i.e, $CII_{v,t=2023}^{req}$.), highlighted in red, alongside the relationship between vessel Dwt and observed CO_2 emissions per Dwt ton-mile.

Figure 1 reveals two main insights. First, vessel operational carbon intensity improvement vary in meaningful across containerships. To avoid a "D" or an "E" rating, vessels need to achieve an average CO_2 reduction of 8.9%, which includes vessels with "A-C" ratings. For vessels with "D" or "E" ratings, the average reduction required is 15.9%. Second, vessel size is an excellent predictor of observed carbon intensity, as evidenced by a simple linear model estimated on the THETIS sample (standard errors reported below coefficients):

$$\ln\left(\overline{CII}_v^{obs}\right) = \underset{(0.04)}{7.62} - \underset{(0.004)}{0.49}\ln(Dwt_v) + \epsilon_v \quad , \quad (R^2 = 0.87; \text{N Obs} = 1903). \tag{1}$$

This model explains 87% of the variation in log-transformed observed carbon intensity. Given the strong explanatory power of Dwt, we aim to estimate the $CII_{v,t}^{obs}$ for vessels outside of the THETIS sample. To do this, we adopt a training and testing approach. We randomly divide our THETIS sample into a training dataset (80% of the sample) and a testing dataset (20% of the sample) 10,000 times. For each iteration, we fit a simple linear model similar to Equation (1), and calculate the in-sample and out-of-sample R^2 and RMSE.

We also adjust fitted values to account for the fact that $CII_{v,t}^{obs}$ in levels is obtained by exponentiating fitted values that are expressed in logs.[8] Our in-sample R^2 based on levels for our chosen

[8] This adjustment is referred to as Duan's smear. Intuitively, it adjusts for the fact that the expected value of the exponentiated log-fitted value differs from the expected value. In our case was approximately ≈ 1.02, see Duan (1983) for a detailed explanation.

model is 0.818 with a 95% CI of [0.754, 0.877]. Standard errors are derived using 10,000 bootstrapped samples. Furthermore, our out-of-sample R^2 based on levels is 0.883 with a 95% CI of [0.860,0.907].

To select our predictive model, we choose the slope term with the highest frequency in 10,000 trials. Notably, the model's coefficient matches Equation (1). With this model, we estimate the $CII^{obs}_{v,t} = \widehat{\overline{CII}}^{obs}_{v}$ and assign letter grades to the remaining vessels.

2.1 Calculating the required slow-steaming in response to IMO2023

Compliance for letter grades D and E vessels, based on IMO2023 requirements, poses a significant challenge. Container ship carbon abatement has so far been achieved through three channels: (1) adoption of lower carbon content fuels; (2) incorporation of more fuel-efficient ship designs; and (3) construction of larger vessels. Of these channels, the first two offer limited potential for lasting environmental improvement: Alternative fuel sources, such as liquefied natural gas and methanol, release comparable carbon emissions over their lifetime use, and reductions achieved through vessel design are only realized when vessels operate at slow speeds (Winnes et al., 2015). Consequently, both the IMO and industry practitioners highlight slow steaming, i.e., speed reduction, as the primary approach for complying with IMO2023.[9]

In order to assess the impact of IMO2023 on vessel speed, we utilize a naval engineering formula from Corbett et al. (2009) to express the per trip fuel consumption F of a vessel as a function of its speed:

$$F_{ijv}(s_v) = \left[F_v^{\text{Main}}\left(\frac{s_v}{s_v^{\text{Des}}}\right)^3 + F_v^{\text{Aux}}\right]\frac{d_{ij}}{24 s_v}, \tag{2}$$

[9] ZIM's executive vice president, Xavier Destriau, noted in an August 2021 interview with Szakonyi (2021) that reducing carbon emissions requires changes in engine power and vessel speed. That means the industry is going "to need more vessels to handle the same amount of cargo," he said. This sentiment was echoed by Gulfstream Shippers Association's President, Garret Bowman, who predicts that many ships will slow down in response to IMO2023 (Slaughter, 2022). Some naval engineers have raised concerns about the effectiveness of this measure, noting that each vessel's engine has a rated speed for optimal efficiency, and recalibrating this speed for existing vessels may not be feasible (Sanguri, 2023). While this could potentially impact fuel efficiency and compliance with new regulations, for the purposes of this paper, we focus on the broader policy implications and assume that recalibration is either feasible or does not significantly affect the outcome. Future research could address this issue more thoroughly.

where F_v^{Main} and F_v^{Aux} are vessel v's main and auxiliary engine fuel consumption per day, respectively; s^{Des} and s_v are v's design and operational speeds, respectively; and d_{ij} is the total distance of the ij route defined by the U.S. importing Customs District i and the exporting country j. We then calculate the ratio of fuel consumption for a vessel slowing down to meet the IMO requirements to s_v^{IMO} relative to operational speed s_v assuming $s_v^{\text{IMO}} = \rho_v s_v$, where $\rho_v \equiv s_{2v}/s_{1v} \leq 1$ represents the reduction in speed necessary for a vessel to meet new operational efficiency standards:

$$\frac{F_{ijv}(s_v^{\text{IMO}})}{F_{ijv}(s_v)} = \frac{F_v^{\text{Main}}(\rho_v s_v / s_v^{\text{Des}})^3 + F_v^{\text{Aux}}}{\rho_v (F_v^{\text{Main}}(s_v / s_v^{\text{Des}})^3 + F_v^{\text{Aux}})}. \tag{3}$$

Given that vessel CO_2 emissions are directly proportional to fuel consumption, comparing the fuel consumption at different speeds allows us to estimate the change in CO_2 output (per ton-mile). We then use the IMO's $CII_{v,t}^{req}$ operational efficiency standard to calculate the slowdown factor ρ_v required for vessels with a "D" or "E" rating to achieve a "C" grade or higher. To find the appropriate slowdown adjustment ρ_v, we minimize the function $H(\rho_v)$, defined as

$$H(\rho_v) \equiv \Big[\frac{F_v^{\text{Main}}(\rho_v s_v / s_v^{\text{Des}})^3 + F_v^{\text{Aux}}}{\rho_v (F_v^{\text{Main}}(s_v / s_v^{\text{Des}})^3 + F_v^{\text{Aux}})} - \Big(1 - \Big(\frac{\overline{CII}_v^{obs}}{\overline{CII}_v^{req}} - 1.07\Big)\Big)\Big]^2. \tag{4}$$

where the minuend comes from equation (3), while subtrahend comes from comparing a vessel's current operational rating to its IMO2023 standard (see Table 2). We subtract 1.07 because a +7% deviation is the maximum allowed for a vessel to still receive a "C" grade. For vessels with multiple observations, we use average values. We minimize the squared difference between the required IMO2023 improvements (minuend) and the speed-induced relative change in fuel consumption (subtrahend). This ensures the necessary CO_2 reductions are achieved, balancing speed and efficiency. For vessels currently rated "C" or better, we set $\rho_v = 1$.

To use equation (3), we require data on container ship routes, vessel speeds, fixed technical characteristics (main engine fuel consumption, auxiliary fuel consumption, and design speed), and observed operational carbon intensity $CII_{v,t}^{obs}$. We identify U.S.-bound container ships using Panjiva bill

of lading data and BlueWater Reporting ship rotation data, and calculate vessel operational speeds using THETIS-MRV and BlueWater Reporting data. Fixed technical characteristics are measured or imputed using Clarkson's WFR data, and missing values of $CII^{obs}_{v,t}$ are measured or imputed based on the relationship between vessel size and operational carbon efficiency captured by equation (1).[10]

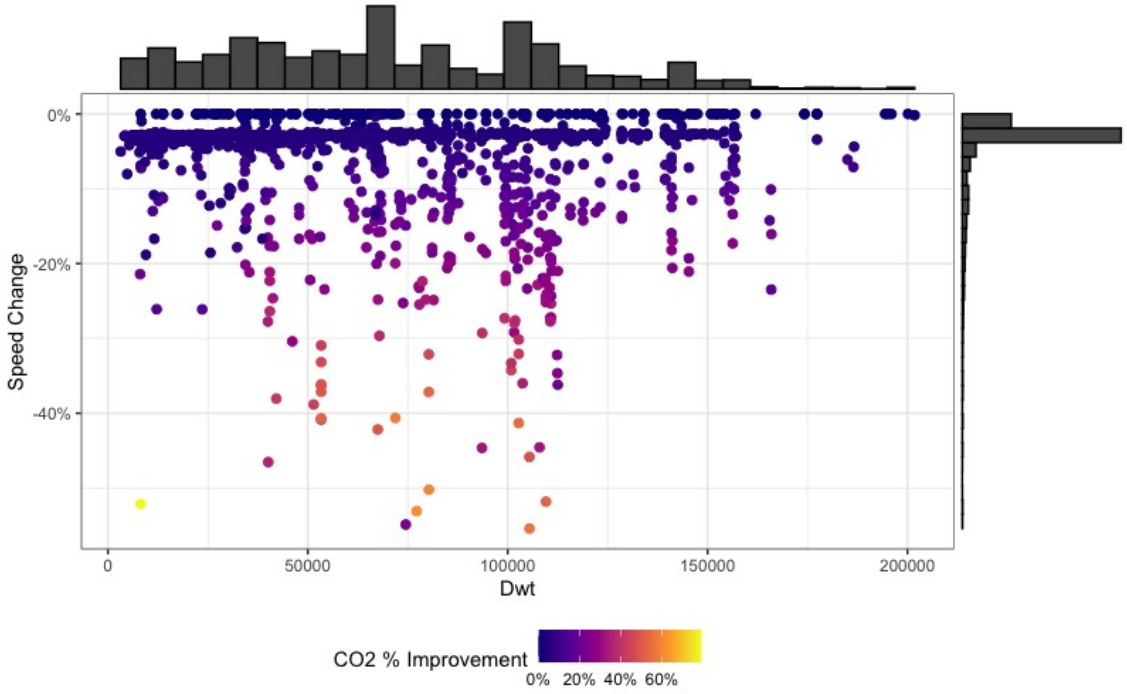


Figure 2: IMO2023 slowdown calculations (ρ_v)
Notes: The unit of observation in this Figure is a vessel. The horizontal axis corresponds to deadweight tonnage (a measure of vessel size) whereas the vertical axis corresponds to how much a vessel needs to slow down (e.g. ρ_v) in percentage terms to meet IMO2023 standards. The unweighted marginal densities of both vessel size and slowdown are plotted alongside the appropriate axis. Each vessel/point is colored according to how much the slowdown will improve the vessel's operational efficiency rating: brighter (darker) colors correspond to greater (lesser) operational efficiency improvements.

In Figure 2, we present our estimates of vessel slowdown as a function of vessel size measured in Dwt. Each vessel is color-coded according to the size of the carbon operational efficiency increase needed to attain a "C" grade or better. The results highlight significant heterogeneity across vessel size and speed adjustments. On average, the Dwt capacity-weighted vessel slowdown is approxi-

[10] See Online Appendix A.3.1 for details on identifying U.S.-bound container ships, Online Appendix A.3.2 for calculating vessel speed, Online Appendix A.3.3 for modeling technical characteristics, and Online Appendix A.3.4 for imputing $CII^{obs}_{v,t}$. Table A5 summarizes data sources and methods, while Online Appendix A.3.6 provides more details on the speed adjustment factor ρ_v.

mately **5.2%**, leading to a corresponding **7.3%** increase in carbon operational efficiency. When we restrict our attention to vessels that must slow down, the Dwt capacity-weighted average speed reduction rises to 6.4%, with a corresponding 8.7% increase in carbon operational efficiency.

2.2 Calculating effective capacity reduction

We begin by providing suggestive evidence that the assumption of binding capacity constraint accurately describes capacity use in maritime transportation. This step is necessary to establish that slow steaming reduces the effective capacity of the ocean fleet in the short-run due to full utilization and slow vessel construction. We use Clarksons *Shipping Intelligence Network* (SIN) to assess fleet capacity utilization, calculating idle TEU capacity daily between 2014 and 2022. Figure 3 indicates that idle capacity fluctuates between 1.3% and 6.8% within this period, averaging 2-3%. Some instances of idle capacity stem from low demand, port congestion,[11] maintenance, and schedule adjustments. Therefore, we conclude that observed idle rates support full utilization of the containerized ocean fleet.

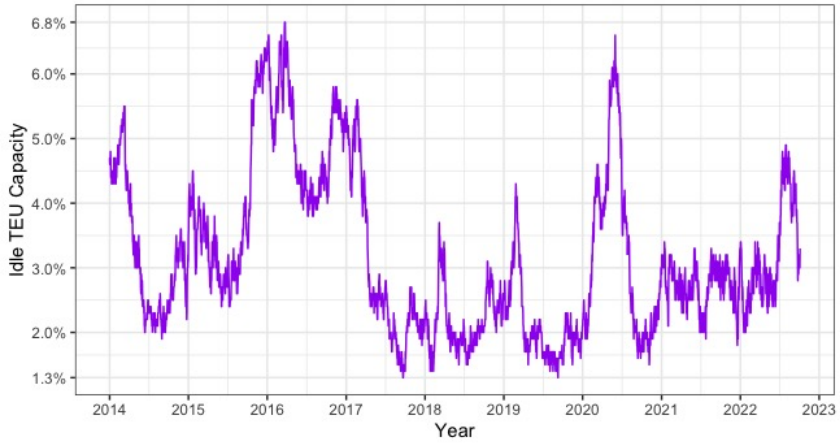


Figure 3: Historic Daily Idle Ocean TEU Capacity
Notes: Figure 3 relies on data from Clarksons Shipping Intelligence Network (SIN).

In the short-run, ocean shipping capacity is constrained, as building a new vessel can take up to three years (Kalouptsidi, 2014; Chokshi, 2020). Therefore, the required slow-down of the ocean fleet

[11] For example, wait times outside of ports may reach up to 22 days at the most congested ports (Thomsen, 2021).

will result in a reduction of ocean fleet capacity. To quantify this effect, we first use the calculated vessel speed reduction ρ_v to determine a more aggregated route-level slowdown, ρ_{ij}, where the route is defined between an exporting country j and an importing U.S. Customs District i.[12] Assuming a representative vessel on route ij, the number of corresponding round trips n_{ij} is

$$n_{ij} = A \Big/ 2 \left(TIME_{ij} + \text{port}(\text{port traffic}_{ij}) \right), \tag{5}$$

where A is the number of sailing days in the year and $TIME_{ij}$ is the average route time.[13] The time spent at port is modeled as a function of port traffic $\text{port}(\text{port traffic}_{ij})$ using Automatic Identification System (AIS) tracking data. AIS does not report time at port for all ports. We overcome this issue by computing the weighted average for the ports where the data are available, namely $\overline{\text{port}}$ =2.53 days, and assign this average to all ports in our sample.[14]

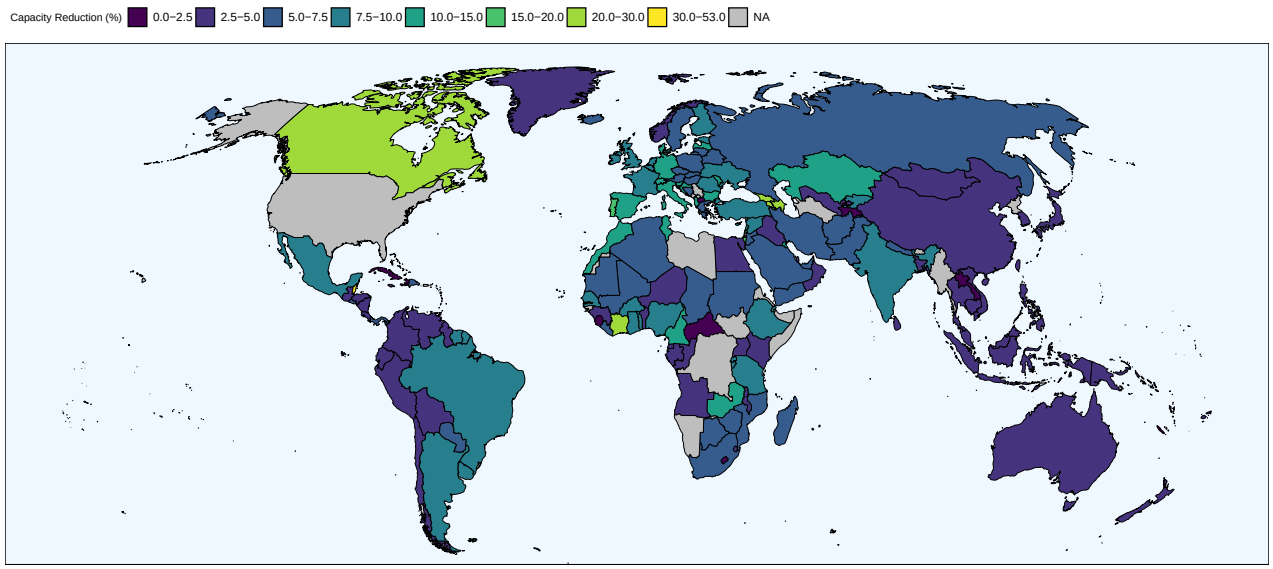
We assume that a vessel's time in port increases with port congestion. Using the same AIS data, we calculate port time to estimate the port time elasticity, κ, with respect to container traffic. Our estimate of $\check{\kappa}$ shows that a 10% increase in port traffic is associated with a 1.97% increase in a vessel's time at port, controlling for vessel, time, and port fixed effects. This estimate comes from Column (4) of Table A7 in Online Appendix A.3.7 and is qualitatively similar to the range of vessel dwell time elasticities reported by Wong and Fuchs (2022).

Reducing vessel speed has two opposing effects in our model. First, it increases the time spent on a route, which reduces the number of round trips and capacity for the year. Second, slower vessels result in fewer vessels in ports, reducing traffic. This, in turn, means that a vessel's time in port is reduced, leading to more round trips and partially restored capacity. Moreover, in the short-run, the relative change in the number of round-trips is equal to the change in relative route capacity. We

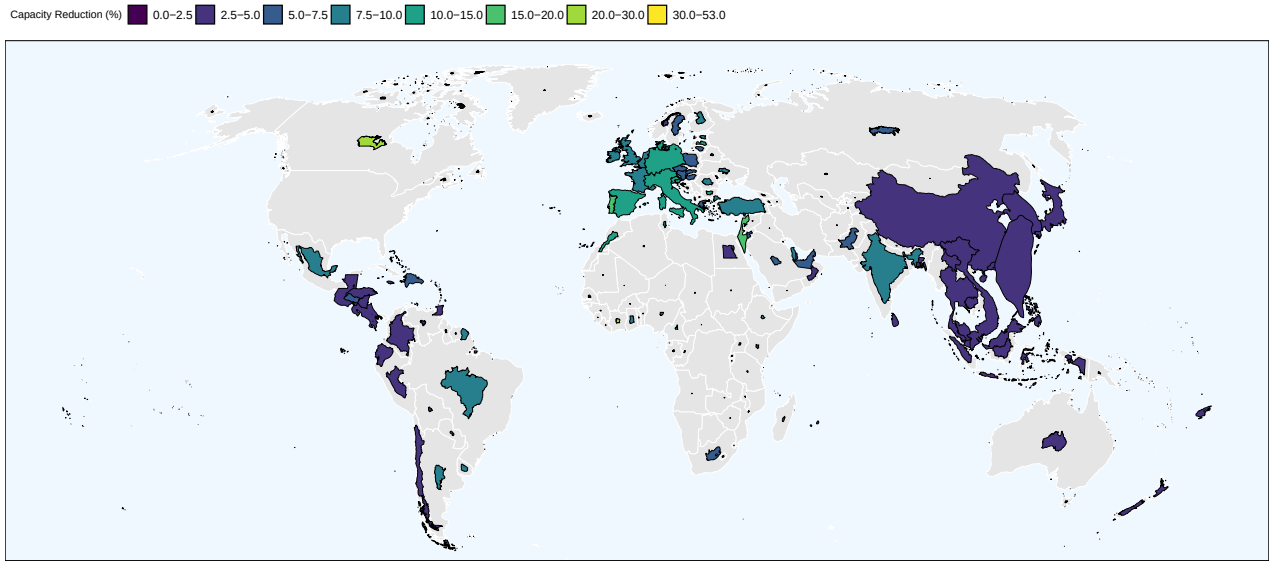
[12] Towards this goal, we map individual vessels to route ij. For details, see Online Appendix A.3.8.

[13] We assume that vessels are active for A =340 days out of the year to reflect off-hire periods or for statutory maintenance, dry docking, etc. This is the number used by Haralambides (2019). Our analysis does not depend on A because we assume that the number of sailing days per year is unaffected by IMO2023.

[14] We use AIS tracking data on container ships serving U.S. ports from Marine Cadastre to estimate time at port and how it depends on traffic. Refer to Online Appendix A.3.7 for more information on data and estimation details.



(a)



(b)

Figure 4: IMO2023 US Capacity Impacts

Notes: Both panels depict changes in country containerized export capacity to the US post IMO2023. Changes in country j's capacity are calculated via $(\sum_i \widehat{q}_{ijc} q_{ijc})/(\sum_i q_{ijc}) - 1$; this calculation informs how we color-code each country. The difference between (a) and (b) is that (b) is cartogram, where country geometries are scaled according to trade volume with the US. In this way, panel (b) shows that East Asian and Western European capacity reductions will be (numerically) more significant.

calculate the change in route ij capacity, $\widehat{q}_{ijc}$ brought on by IMO2023's slower speeds as:

$$\widehat{q}_{ijc} \equiv \frac{n_{ijT}(\rho_{ij})}{n_{ijt}} = \frac{TIME_{ij} + \overline{\text{port}}}{\frac{1}{\rho_{ij}} TIME_{ij} + \overline{\text{port}}\left(\widehat{q}_{ijc}\right)^{\kappa}}, \tag{6}$$

where t and T refer respectively to time periods pre and post implementation of IMO2023. We solve for $\widehat{q}_{ijc}$ numerically. Our aggregated results reveal that IMO2023 will lead to a 5.2% reduction in U.S. imports' capacity and increase the average route shipping times by 0.54 days.[15] The required capacity reduction varies across countries. Figure 4 displays our $\widehat{q}_{ijc}$ calculations aggregated at the level of importing country. For example, Chinese ocean export capacity will decrease by approximately 4.2%, Brazilian export capacity by 8.2%, and German export capacity by over 10.3%.

Our results align with industry reports on the impact of IMO2023 on shipping capacity. For instance, Maersk CEO Søren Skou asserted that the ocean company would require 5-15% more capacity to comply with the regulations due to slow steaming (Mandra, 2022). Similarly, Hapag-Lloyd CEO Rolf Habben Jansen reported that the company would need an extra 5-10% capacity (Kershaw, 2022). Furthermore, our projections regarding decreases in speed and imports align with the findings presented by the U.N. Conference on Trade and Development (UNCTAD, 2021).[16]

2.3 A Note on Enforcement Mechanism

Enforcement of IMO regulations is generally left to member states, and implementation details are often left to MARPOL signatories.[17] For example, in the U.S., MARPOL Annex IV regulations have been incorporated into law by the Act to Prevent Pollution from Ships (APPS) and implemented within 33 USC 1901 and 33 CFR 151 (USCG, 2022). The U.S. Coast Guard enforces maritime emissions standards, including Annex IV's regulations on sulfur content in commercial vessels' bunker fuels (Hansen-Lewis and Marcus, 2022).

Proponents of the IMO's efforts to improve maritime emissions by collaborating with port states,

[15] Using route traffic volumes as weights, we compute both summary statistics as weighted averages. We then compute standard errors via boot-strap with 1,000 replications. Accordingly, we find short-run capacity reductions to have a 95% confidence interval (CI) of [5.34%, 6.40%]. Likewise, short-run shipping time increases have a 95% CI of [0.40 days 0.69 days]. Additional boot-strap standard errors/confidence intervals for other summary statistics are available upon request.

[16] Specifically, with their HIGH scenario results as reported in Table 1. UNCTAD's analysis includes all modes of ocean transportation, including liner, dry-bulk, tankers, and ro-ro, and offers a broad geographical coverage.

[17] MARPOL stands for "International Convention for the Prevention of Pollution from Ships, 1973 as modified by the Protocol of 1978" and is one of the world's most significant international marine environmental conventions; see the U.S. Coast Guard's summary page here.

i.e., MARPOL signatories, highlight the success of IMO2020. That set of regulations lowered the maximum sulfur content in fuel used by vessels outside of emission control areas from 3.5% m/m to 0.50% m/m. Even after accounting for the reduction in commercial freight traffic due to COVID-19, IMO2020 was a success, resulting in a 46% reduction in SO_2 aerosol volume (Yuan et al., 2022).[18]

Despite the success of IMO2020, effective enforcement of emissions regulations for both owners and charters remains a challenge, which may delay the implementation of IMO2023 (Kinyua, 2023). The Baltic and International Maritime Council (BIMCO) has created a contractual framework called the "CII Operations Clause for Time Charter Parties," which purports to facilitate cooperation between shipowners and charters to achieve the IMO2020 carbon intensity goals. However, the "Clause" does not transfer regulatory responsibility for compliance to charters, and it is the shipowners who will ultimately be accountable for meeting IMO2023 compliance requirements. As a result, charters have little incentive to adopt the "Clause" (Keys, 2022a). Keys (2022b) suggests that the real enforcement of IMO2023 may come from a vessel's flag state's ability to issue or withhold a Statement of Compliance: vessels without "SoC" are unchartable.[19]

3 Model

Our model examines the substitutability between air, land, and ocean transportation for international imports across regions within a country. While Hummels and Schaur (2013) focused on substitution between ocean and air transport, we expand this by including land transport and competition with domestic production. Unlike their product-specific approach, our model aggregates total demand across transportation modes. For instance, a rise in ocean freight rates for imported cars may increase demand for air-transported watches. This cross-product substitution could amplify the ocean-to-air

[18] The remaining concern is that IMO2020 still permits the use of open-loop scrubbers, which discharge sulfur into the sea, contributing to ocean acidification—a significant environmental issue (International Maritime Organization, 2020).

[19] Adopting 'flags of convenience' is common in international shipping, where vessels are registered in port states with open registries. These countries impose lower taxes and fewer inspections, making them attractive to shipowners (Stopford, 2009). Around 45% of TEU US imports are carried by ships from Liberia, Panama, and Malta, which have open registries; US-registered containerships account only for 5%.

shift compared to Hummels and Schaur (2013).

By way of expositional motivation, it is important to note that the share of imported goods that use multiple transport modes represents an economically significant share of imported goods. Using U.S. Census data by transport mode, Figure 5a shows that there are thousands of HS10 products that are transported by both air and containership. Moreover, Figure 5b shows that from 2012 - 2022, a growing share (by weight) of products imported by both air and containership are products that can be transported by either mode: this share of imports rose from about 23% in 2012 to about 30% by 2022. Likewise, the value of share of such bi-modal imported products ranged from 33% to about 40% over the same period. Furthermore, over the same time period, approximately 30.4% and 36.8% of all products imported by air and containership by weight and by value, respectively, were products that could be transported by either mode.[20]

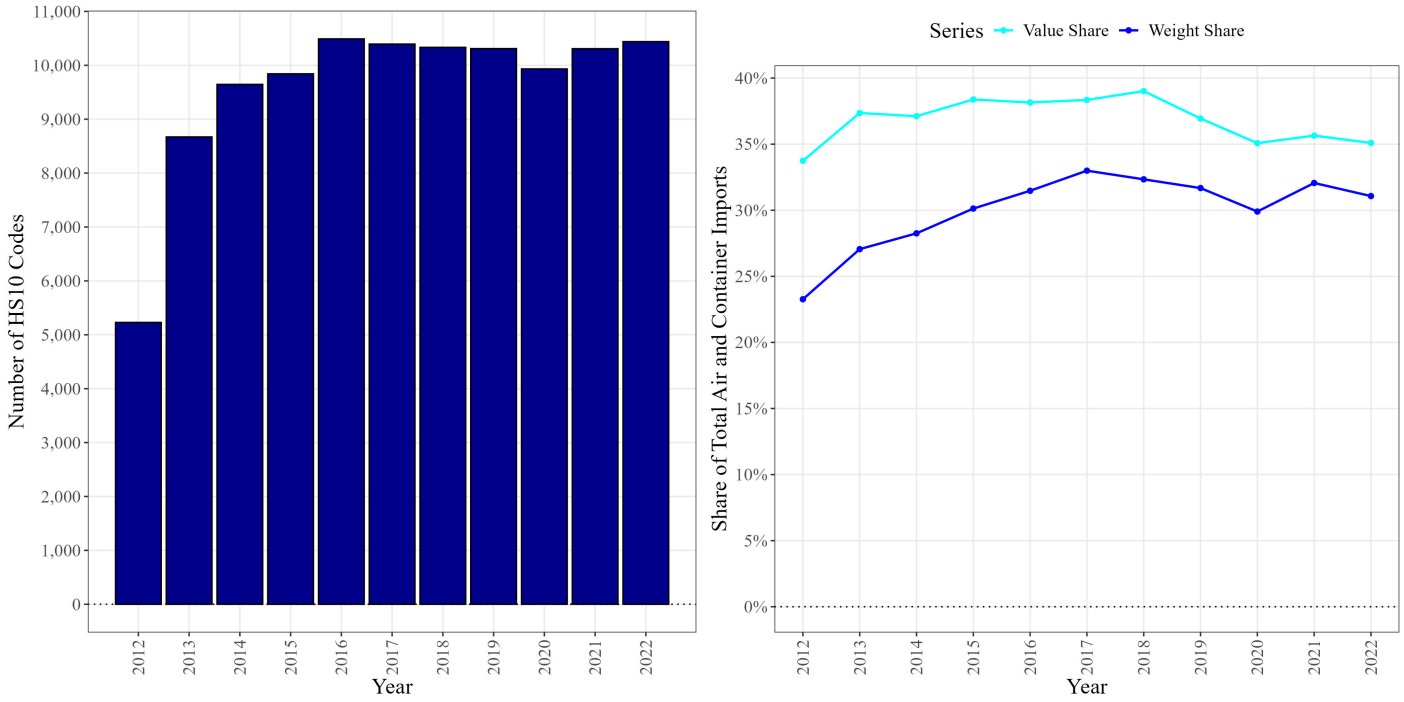
3.1 Environment

The model is set from the perspective of one country, Home, which consists of multiple custom districts indexed by i and imports foreign goods from $j = 1, 2, ..., J$ foreign countries via three modes of transportation indexed by m: air, land, and ocean. Not every ij is connected by all three modes; the set of modes for each ij is exogeneously given and denoted by M_{ij}.

Preferences. Consumers have Cobb-Douglas preferences defined over a non-manufacturing numeraire good 0 and composite differentiated good. Differentiation is based on the national origin j[21] and goods' mode of transportation: air, land, and ocean, where mode of transportation is viewed as a proxy for various product characteristics, including its density, value per unit, and product's time sensitivity, as previously highlighted by Hummels and Schaur (2013). Formally, a Home's represen-

[20] We use US import data provided by Peter Schott's website. We define an HS10 bimodal product (i.e., a product that is imported by both air and containership) if a given HS10 product has non-zero import value for a given year and exporting country - importing U.S. Custom District route. In this way, Figure 5 depicts HS10 products imports for goods that are transported by both air and containership for a *trade-route-year* as opposed to all imports that enter into the United States in a given year that are transported by both air and containership. We focus on products that are delivered by both air and containership because we do not have access to data on HS10 product level land based imports.

[21] The national origin, or Armington, differentiation is quite common in trade literature and has also been used in the related paper on emissions from transportation of traded goods by Shapiro (2016).



(a) Number of HS10 Products

(b) Import Shares

Figure 5: HS10 Products Transported by both Air and Containership 2012-2022

tative consumer in district i and year t maximizes the following utility function:

$$\begin{aligned} \max_{q_{ijmt}} U_{it} &= q_{0,it}^{1-\mu}\left(Q_{iit}^{\frac{\sigma-1}{\sigma}}+\sum_{j\neq i}Q_{ijt}^{\frac{\sigma-1}{\sigma}}\right)^{\mu\frac{\sigma}{\sigma-1}} \quad , \quad \sigma>1 \\ \text{s.t. } & q_{0,it}+P_{iit}Q_{iit}+\sum_{j\neq i}P_{ijt}Q_{ijt}=I_{it}, \end{aligned} \tag{7}$$

where $q_{0,it}$ is the non-manufacturing composite good 0;

I_{it} is the overall budget for district i in year t;

q_{ijmt} and p_{ijmt} are the quantity and price of good m imported by i from j in year t;

P_{ijt} and Q_{ijt} denote origin j-destination i-year t-specific price and quantity indexes given by

$$Q_{ijt}=\left(\sum_{m\in M_j}v_{jmt}q_{jmt}^{\frac{\varepsilon-1}{\varepsilon}}\right)^{\frac{\varepsilon}{\varepsilon-1}} \quad \text{and} \quad P_{ijt}=\left(\sum_{m\in M_j}v_{jmt}^{\varepsilon}p_{ijmt}^{1-\varepsilon}\right)^{\frac{1}{1-\varepsilon}} \quad , \quad \varepsilon>\sigma>1, \tag{8}$$

where P_{iit} and Q_{iit} denote local price and quantity of the manufacturing good in district i;

ν_{jmt} denotes the exporter-mode-year-specific preference shifters. For imports transported by sea, the magnitudes of these shifters, among other things (captured by ϑ_{jt}), depend on the delivery time, which is a function of the average distance from country j, d_j, speed per hour s_j, and time spent in port:

$$\nu_{jmt} = \vartheta_{jt}(d_j/(24s_j) + \overline{\text{port}})^{\beta_k} \qquad \vartheta_{jt} > 0, \quad \beta_k < 0. \tag{9}$$

Production of Goods and Transportation. Following Hummels et al. (2009), we express the delivered prices of imported goods imported by i from j via transportation mode m in year t, and denoted by p_{ijmt}, as a function of the free-on-board (FOB) price p^{FOB}_{ijmt}, iceberg tariff $\tau_{ijmt} \geq 1$, and specific transport cost f_{ijmt}:

$$p_{ijmt} = p^{\text{FOB}}_{ijmt}(\tau_{ijmt} + f_{ijmt}/p^{\text{FOB}}_{ijmt}) \tag{10}$$

To keep our model tractable, we simplify it by abstracting away from critical issues that affect ocean freight rate formation, including port efficiency (Blonigen and Wilson, 2008), average vessel size (Asturias, 2020), average unit values (Hummels and Skiba, 2004), geography and networks in ocean transportation (Ganapati et al., 2020), and backhaul effects (Ishikawa and Tarui, 2018; Wong, 2020).[22] Instead, we focus on such determinants of the freight costs as the number of carriers (Hummels et al., 2009; Ardelean and Lugovskyy, 2023), fuel and non-fuel costs components, speed (s_{ij}), and time spent in ports. Following Hummels et al. (2009), we assume that, on each route ij, a fixed number of containerized ocean carriers, N_{ij}, compete in quantities à la Cournot. Each ij transportation market is treated as a segmented market with all carriers in ij having access to the same symmetric technology. The technology is characterized by an annual fixed cost of Z_{ij} and a marginal cost per trip of c_{ij}, which consists of fuel and non-fuel cost components:

[22] We justify this assumption in the estimation section by stating that these determinants are already incorporated into the observed freight rates. When analyzing policy-induced changes, we assume that any changes to these determinants resulting from the policy will have a secondary effect on freight rates compared to the policy's direct impact.

$$c_{ij} = b_{ij}F_{ij}(s_{ij}) + D_{ij}((d_{ij}/24s_{ij}) + \overline{\text{port}}), \tag{11}$$

where b_{ij} is the bunker fuel price, F_{ij} is the fuel amount per trip, previously defined by equation (2), d_{ij} is distance between i and j, and s_{ij} is speed per hour, and D_{ij} daily non-fuel costs (i.e., labor costs, financing costs, etc.).

Based on the evidence presented in Section 2.2, we assume that ocean transportation is operating at full capacity.[23] A similar assumption is less justifiable for air transportation, where on average only 24.3% of payload is used to transport cargo with most of the under-utilized capacity coming from the passenger airplanes (Besedeš and Murshidb, 2022).[24] We confirm these statements, using Domestic and International Segment T100 Traffic Data, by plotting the utilized air capacity over time and across airplane types in Figure 6. Therefore, in our model, we assume that air transportation is subject to significant excess capacity and thus air freight rate may not be affected by demand shocks.

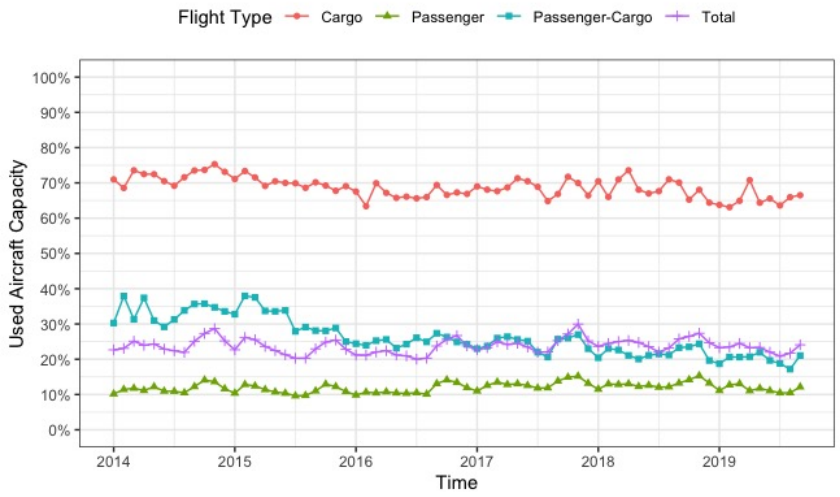


Figure 6: US Air Import Capacity Utilization Over Time

Notes: Figure 6 relies on Domestic and International Segment T100 Traffic Data reported by U.S. and Foreign Carriers and provided by the Bureau of Transportation Statistics (BTS). The Figure shows percentages of utilized cargo capacity in cargo, passenger, and cargo-passenger airplane types.

[23] Leading liner companies, such as Maresk, maintain their own airplane fleet to allow for additional freight capacity. See News (2021).

[24] Passenger airplanes are responsible for 44% of cargo transported by air (Budd and Ison, 2017).

On the definition of a route. To introduce the theoretical notion of a route into our empirical and computational exercises we define route ij as a combination of a U.S. Customs District i and origin country j. This definition matches our focus on the IMO policy which applies to international transportation. By defining a route as only the international portion of the entire journey from the factory floor to the location of final consumption we also avoid loosing tractability due to introduction of inter-route competition and multi-modal transportation. This definition matches the model of competition where several modes can be used to deliver goods between two location. Furthermore, our definition has the advantage that we can meet the data requirements for the cost of transportation and product prices by route and mode with available data sources.

3.2 Equilibrium Demands and Ocean Freight Rates

Without loss of generality, let us focus on district i in year t, which would allow us, for the sake of brevity, we to omit subscripts it. We will proceed by formulating our key results in a form of propositions with their proofs are provided in Online Appendix A.4.

Lemma 1. *The equilibrium demand for imports from country j via mode m can be expressed as*

$$q_{ijmt} = \nu_{jmt}^{\varepsilon\frac{\sigma-1}{\varepsilon-1}} p_{ijmt}^{-\sigma} \lambda_{ijmt}^{\left(1-\frac{\sigma-1}{\varepsilon-1}\right)} P_{it}^{\sigma} Q_{it} \qquad \textit{where} \qquad \lambda_{ijmt} = \frac{p_{ijmt} q_{ijmt}}{\sum_{m \in M_{ijt}} p_{ijmt} q_{ijmt}} \tag{12}$$

denotes the expenditure share of imports by mode m in total imports from origin j.

Proof. See Online Appendix A.4. □

The functional form we use is fairly standard compared to other trade models with nested CES and Armington differentiation. Specifically, as in Khandelwal (2010); Lashkaripour and Lugovskyy (2023), it features origin-specific differentiation at the upper nest and product differentiation within the mix of goods from a given origin at the lower nest. However, previous nested models did not focus as much on the transportation sector. Therefore, we are the first to derive the equilibrium (per-unit) freight rate for this model and demonstrate how it relates to other established models.

Lemma 2. *The equilibrium per-unit freight rate f_{ijct} under nested CES preferences, constant marginal cost of transportation c_{ijct}, and n_{ijct} carriers competing à la Cournot on a given route ij is given by:*

$$f_{ijct} = \left(\frac{\tilde{\epsilon}}{\tilde{\epsilon}-1}\right) c_{ijct} \quad with \quad \tilde{\epsilon} \equiv \underbrace{\underbrace{\underbrace{\underbrace{\varepsilon}_{\substack{CES\ with \\ an\ advalorem\ \tau}} \times n_{ijct}}_{\substack{CES\ with\ an\ ad\ valorem\ \tau\ and \\ Cournot\ oligopoly\ with\ n\ firms}} \times \frac{f_{ijct}}{p_{ijct}}}_{Hummels\ et\ al.\ (2009):\ CES,\ Cournot,\ per\text{-}unit\ f}}_{\substack{This\ paper:\ Hummels\ et\ al.\ (2009)\ with\ nested\ CES: \\ Armington\ and\ inter\text{-}modal\ substitutability}} \times \left(1 - \lambda_{ijct}\left(1 - \frac{\sigma}{\varepsilon}\right)\right) \tag{13}$$

where λ_{ijct} is a share of manufacturing imports transported by the container ships.

Proof. See Online Appendix A.4. □

The intuition for Lemma 2 can be seen by noting that equation (13) is derived from the standard markup expression $f_{ijct} = \left(\frac{\tilde{\epsilon}}{\tilde{\epsilon}-1}\right) c_{ijct}$, where $\tilde{\epsilon}$ is the elasticity of shipping demand with respect to shipper's per unit freight rate f_{ijct}. While this is a standard markup, the specific determinants of the elasticity $\tilde{\epsilon}$ depend on the model. In the simplest scenario involving an ad valorem freight rate, the elasticity $\tilde{\epsilon}$ equals ε. However, as outlined by Hummels et al. (2009), if we introduce Cournot competition with n_{ijct} shippers and incorporate a per-unit freight rate, the elasticity must be adjusted. The presence of multiple competitors reduces the markup, necessitating an adjustment by n_{ijct}. Additionally, the share of transportation costs in the delivered price affects demand responsiveness; a smaller transportation cost share dampens this responsiveness.

Furthermore, when we introduce nested CES preference structure the elasticity requires an additional adjustment by $\left(1 - \lambda_{ijct}\left(1 - \frac{\sigma}{\varepsilon}\right)\right)$. To illustrate the intuition, consider two limiting values of λ_c—the share of containerized transportation in manufacturing imports. If λ_c is negligible (i.e., approaches zero), the influence of the upper nest is minimal. Conversely, when $\lambda_c = 1$, the lower nests effectively disappear as all shipments are made using containers, causing σ to replace ε. In all interior scenarios, elasticity increases with $\frac{\sigma}{\varepsilon}$ and decreases with λ_c. We will use these results to outline the implications the short-run and long-run results in Sections 5 and 6. For the welfare changes,

we will apply hat algebra to the indirect utility function, as detailed in the following Lemma.

Lemma 3. *Changes in welfare can be approximated using hat algebra as follows:*

$$\widehat{W}_i = \left[\psi_{iit}\widehat{P}_{iit}^{1-\sigma} + \sum_{j\neq i}\psi_{ijt}\widehat{P}_{ijt}^{1-\sigma}\right]^{\frac{-\mu}{1-\sigma}} \tag{14}$$

where $\widehat{X}$ represents the proportional change in X between period t and the new time period T, i.e., $\widehat{X} = \frac{X_T}{X_t}$. The terms ψ_{iit} and ψ_{ijt} denote the shares of products iit and ijt in the consumption of manufacturing goods in region i.[25]

Proof. See Online Appendix A.4. □

4 Estimating and Calibrating Model Parameters

In this section, we structurally estimate and calibrate the model parameters, which we will then use to evaluate the effects of IMO2023. Our analysis will focus on U.S. imports, as detailed data on import prices and freight rates by mode of transportation are limited for other countries. Based on theory, the evaluation of IMO2023 requires estimates for the within-nest and across-nest elasticities, ε and σ, as well as the district-exporter-mode-time preference parameters, ν_{ijmt}. Our estimation follows the established methodology for nested CES utility functions (e.g., Khandelwal, 2010; Levchenko et al., 2011; Lashkaripour and Lugovskyy, 2023). Table 3 summarizes datasets used in this Section.

4.1 Data Sources

For demand estimation, we use three datasets. To construct the quantity and unit values (prices) of goods imported by air and vessel, we rely on monthly U.S. Census import data from 2011-2022.

[25] Based on the definition of consumption share of manufacturing, ψ_{iit}, and the following equality based on our definition of utility, $Q_{ijt}P_{ijt} = Q_{iit}P_{iit}\left(\frac{P_{ijt}}{P_{iit}}\right)^{1-\sigma}$, one can show that $P_{iiy} = \left(\frac{\psi_{iit}}{1-\psi_{iit}}\sum_{j\neq i}P_{ijt}^{1-\sigma}\right)^{\frac{1}{1-\sigma}}$ and $Q_{iit} = \frac{\sum_{j\neq i}Q_{ijt}P_{ijt}}{P_{iit}^{\sigma}\left(\sum_{j\neq i}P_{ijt}^{1-\sigma}+P_{iit}^{1-\sigma}\right)-P_{iit}}$.

Table 3: Datasets Used in Estimating and Calibrating Model Parameters

Name of the Dataset	Key Variables	Purpose of Using the Dataset	Section
U.S. Census Import Data	Freight charges (USD), import values (USD), import weight (kg) by mode (e.g., vessel containerized, air)	To estimate freight-mode specific demand and calculate ad-valorem freight costs for import routes	4.1
World Integrated Trade Solution (WITS)	Annual country-HS6 level U.S. import tariff data	To compute mode-route-time tariffs as part of the weighted average used in freight demand estimation	4.1
TransBorder Freight Data by U.S. Dept of Transportation	Import values, weight, and charges by HS2 commodity from Canada and Mexico to U.S. Customs Districts	To account for land freight charges, especially for imports from Canada and Mexico	4.1
BlueWater Reporting	Number of carriers per route	To estimate the number of carriers for calculating marginal costs of freight rates	4.2

These data are mode-specific (e.g., containerized vessel, non-containerized vessel, air), reported at the HS6 level, and specify the U.S. Customs District of entry and the exporting country. For containerized vessel and air shipments, we observe freight charges (USD), import values (USD), and import weight (kg).

Since the U.S. Census Imports dataset does not cover land transportation, we use the TransBorder Freight Data from the U.S. Department of Transportation. These data report import values, weight, and charges by HS2 commodity for imports from Canada and Mexico to U.S. Customs Districts.

For air and ocean imports, we first aggregate data by mode, route, time, and HS6 codes to generate freight charges, import values, and import weight. We then integrate U.S. import tariff data from WITS at the HS6 level and use it to calculate mode-route-time tariffs (τ_{ijmt}), employing HS6 value shares for weighting. Finally, we sum over HS6 codes to produce the mode-route-time data used for estimation, aggregated to a quarterly time frequency. Factory prices (p_{ijmt}^{FOB}) are defined as the ratio of import values to weight, unit freight charges (f_{ijmt}) as freight charges to weight, and ad-valorem freight costs as their ratio.

For land transport, we use WITS data to compute value-weighted tariffs at the HS2 level for imports from Canada and Mexico. We then aggregate this data to obtain the country-district quantity and prices for land imports.

4.2 Estimating Demand Parameters in the Benchmark Model

We estimate the key parameters of our model by using our theoretical demand equation (12). We log-linearize it: $\ln q_{ijmt} = \varepsilon\frac{\sigma-1}{\varepsilon-1}\ln \nu_{jmt} - \sigma \ln p_{ijmt} + \left(1 - \frac{\sigma-1}{\varepsilon-1}\right)\ln \lambda_{ijmt} + \ln P_{it}^{\sigma} Q_{it}$, and estimate:

$$\ln q_{ijmt} = \theta_{jmt} + \beta_1 \ln p_{ijmt} + \beta_2 \ln \lambda_{ijmt} + \theta_{it} + \mu_{ijmt}, \tag{15}$$

where $\theta_{jmt} \equiv \varepsilon\frac{\sigma-1}{\varepsilon-1}\ln \nu_{jmt}$ and $\theta_{it} \equiv \ln P_{it}^{\sigma} Q_{it}$ can be treated as fixed effects; and μ_{ijt} is the error term. Equation (15), while using different less granular definition of variety within a nest, has strong similarities with the estimation equation (15) of Lashkaripour and Lugovskyy (2023).

In order to address the potential endogeneity concerns with prices and shares we follow typical approach used notably by Khandelwal (2010) and Levchenko et al. (2011). We instrument prices p_{ijmt} with unitary "cost insurance freight" (CIF) charges f_{ijmt} and cross product of route distance DIST_{ij} with West Texas Intermediate (WTI) crude oil price. The shares λ_{ijmt} are instrumented with the number of HS 10 categories within a given mode route and year, $ijmt$. Table 4 presents both the OLS and IV estimates (including the first stage of the IV):

Table 4: Results of Estimating (15)

	OLS	First Stage		Second Stage
Dependent Variable	$\ln(x_{ijmt})$	$\ln(p_{ijmt})$	$\ln(\lambda_{ijmt})$	$\ln(x_{ijmt})$
	(1)	(2)	(3)	(4)
$\ln(p_{ijmt})$	-0.911^{***}			-1.282^{***}
	(0.009)			(0.017)
$\ln(\lambda_{ijmt})$	0.735^{***}			0.903^{***}
	(0.007)			(0.047)
$\ln(f_{ijmt})$		0.458^{***}	-0.066^{***}	
		(0.009)	(0.008)	
$\ln(\text{DIST}_{ij} \times \text{WTI}_t)$		0.232^{***}	0.493^{***}	
		(0.024)	(0.035)	
Num of HS10_{ijmt} within $ijmt$		0.074^{***}	0.640^{***}	
		(0.009)	(0.038)	
Num. obs.	95,139	94,893	94,893	94,893
R^2	0.855	0.751	0.286	0.843
FE: (it)	504	504	504	504
FE: (jmt)	4,978	4,977	4,977	4,977

Notes: $^{***}p < 0.01$; $^{**}p < 0.05$; $^{*}p < 0.1$

We then identify $\breve{\sigma} = -\breve{\beta}_1$, $\breve{\varepsilon} = 1 - \frac{\breve{\beta}_1 - 1}{\breve{\beta}_2 - 1}$. Table 5 reports the elasticity results. The upper-case elasticity of substitution $\hat{\sigma}$ is 0.911 for OLS and 1.282 for IV, respectively. The lower-case elasticity of substitution $\breve{\varepsilon}$ is 4.440 for OLS and 14.279 for IV, respectively. Both estimates are statistically significant at 1% level. For comparison, in Lashkaripour and Lugovskyy (2023) the IV estimate of σ in the pooled regression for manufacturing is 3.766 and of ε is 9.135.[26]

Table 5: Elasticity Results based on Table 4

Parameter/Model	OLS		IV (2SLS)	
	est	std.error	est	std.error
σ	0.911	0.009	1.282	0.017
ε	4.440	0.033	14.279	1.374

Notes: Standard errors are derived via the Delta-method.

From Table 4, we also recover ν_{jmt} by $\breve{\nu}_{jmt} = \exp\left(\breve{\theta}_{jmt}/\breve{\varepsilon}\frac{\breve{\sigma}-1}{\breve{\varepsilon}-1}\right)$. To show that preferences for timely delivery change as a result of delivery time, we estimate the following equation:

$$\log\left(\frac{\breve{\nu}_{\text{air},jt}}{\breve{\nu}_{\text{cnt},jt}}\right) = \beta_\nu \log(\text{Sea Time}_{jt}) + \vartheta_t + \epsilon_{jt}$$

Note that sea time includes 2.53 days in port and the regression model below uses total container import volume for jt as weights. Towards this goal, we utilize annualized 2012-2019 BlueWater data on the average number of days in transit for every route j (including 2.53 days in port), which we label as Sea Time$_{jt}$. Table 6 presents the results. An intuitive interpretation of these estimates is that for a given U.S. region i, a 1% increase in the ocean travel time is associated with a β_k% decrease in the preference parameters for ocean transportation. In practice, this marginal effect translates into a 0.318% to 0.267% decreases for the unweighted and weighted IV regressions, respectively.

[26] Their results are reported in their Online Appendix S1. Our elasticities are expected to be of different magnitudes due to the different levels of aggregation within nests. Specifically, our definition of a "variety" within a nest includes all goods transported from j to i using a given mode of transportation, where i represents a customs district in the U.S. In contrast, their definition included all goods shipped by a given firm in j, regardless of the mode of transportation, to i, where i represents a location in Colombia.

Table 6: Recovering β_ν

	OLS		IV (2SLS)	
Weighted regression?	No	Yes	No	Yes
	(1)	(2)	(3)	(4)
log(Sea Time$_{jt}$)	-1.254^{***}	-1.084^{*}	0.318^{**}	0.267^{*}
	(0.325)	(0.467)	(0.110)	(0.140)
Num. obs.	695	683	695	683
R^2	0.023	0.021	0.012	0.009
FE: (t)	8	8	8	8

Notes: $^{***}p < 0.01$; $^{**}p < 0.05$; $^{*}p < 0.1$

5 Short-Run Effects of IMO2023

In this section, we predict the short-run effects of IMO2023 on carbon emissions from maritime and air transportation of imported goods to the United States. In Section 2, we demonstrated that IMO2023 will decrease the capacity of containerized fleet and calculated these decreases as proportions $\widehat{q}_{ijc} \equiv \frac{q_{ijcT}}{q_{ijct}}$ for each route ij. We take this change in capacity as given in calculating the post-reform equilibrium.[27] For all other variables of interest, we define the proportional change in a similar fashion with $\widehat{X} \equiv \frac{X_T}{X_t}$, where subscripts t and T denote before and after IMO2023, respectively. For brevity, we drop the time subscripts in the remainder of this section. Thus, any variable X refers to its pre-reform value, and $\widehat{X}X$ denotes its post-reform value. We now present Lemma 4, which is the basis for the calculation of short-run effects.

Lemma 4. *In equilibrium, the proportional change in the containerized goods delivered via ocean can be derived as*

$$\widehat{p}_{ijc} = \left(\frac{1}{\widehat{q}_{ijc}} \widehat{P}_{ij}^{\varepsilon-\sigma} \widehat{P}_i^{\sigma} \widehat{Q}_i \right)^{\frac{1}{\varepsilon}}$$

[27] Based on supporting analysis on route stability detailed in Online Appendix A.7, we assume route stability (i.e., there are no changes to the number of routes as a result of the policy reform).

The proportional changes in the air and land delivered imports are given by

$$\widehat{p}_{ijm}(\widehat{p}_{ijc}) = \left(\zeta_m \left(\alpha(\widehat{p}_{ijc}) - 1\right) + 1\right) p_{ijm} \quad \forall m \in \{a, l\},$$

where $\alpha(\widehat{p}_{ijc}) = \dfrac{\widehat{p}_{jc} p_{ijct} + p_{ijct}^{FOB}(1 + \tau_{ijct})}{f_{ijct}}$, *and* ζ_m *is an exogenously set parameter.*

Proof. See Online Appendix A.4. □

For our short-run counterfactual, we abstract from changes in Home's nominal income and, therefore, assume that pre-reform and post-reform expenditures in manufacturing remain unchanged.

$$\widehat{P}_i P_{it} \widehat{Q}_i Q_{it} + \sum_j \sum_{m \in M_{ij}} \widehat{p}_{ijm} p_{jmt} \widehat{q}_{jm} q_{jmt} = P_{it} Q_{it} + \sum_j \sum_{m \in M_{ij}} p_{jmt} q_{jmt} \tag{16}$$

These results allow us to express $\widehat{p}_{ijm}, \widehat{q}_{ijm}, \widehat{P}_{ij}, \widehat{P}_i$, and $\widehat{Q}_i$ as functions of $\widehat{p}_{ijc}$ and define the counterfactual equilibrium as a vector of $\widehat{p}_{ijc}$ for a given $\widehat{Q}_i$. Building on Lemma 4 and the budget constraint (16), we select a value for $\widehat{Q}_i$ and use a fixed-point approach to find $\widehat{p}_{ijc}$ that aligns with this choice, along with all parameters and equations. Stated formally, our problem's objective function is:

$$\min_{\widehat{Q}_i} \left(\frac{\widehat{P}_i P_{it} \widehat{Q}_i Q_{it} + \sum_j \sum_{m \in M_{ij}} \widehat{p}_{ijm} p_{jm} \widehat{q}_{jm} q_{jm}}{P_{it} Q_{it} + \sum_j \sum_{m \in M_{ij}} p_{jm} q_{jm}} - 1 \right)^2 \tag{17}$$

We then verify if the resulting $\widehat{p}_{ijm}(\widehat{Q}_i)$ satisfies the budget constraint. If it does not, we adjust the value of $\widehat{Q}_i$ and repeat the process.

Calculating Carbon Emissions. We use the methodology outlined in Shapiro (2016) to calculate the carbon emissions associated with each mode of transportation. Specifically, we assume an emissions rate of 1439.49 g CO_2 per ton-mile for air transportation on each route.[28] Route air distance is calculated as the great circle distance between the U.S. Customs District i and the country j with the coordinates for country j obtained from CEPII's database. For maritime transportation , we use

[28] This figure is derived from the International Air Transport Association (IATA)'s 2009 fuel economy of air freight transport of 985.97 g CO_2/ton-km, as reported by Shapiro (2016). We convert this figure to ton-miles. Further details can be found in Shapiro's Online Appendix A.4.

route specific CO_2 emissions per ton-mile, calculated based on our shipping data. We estimate ocean mileage based on BlueWater's rotation schedule. We use the great circle distance between the U.S. Custom District i and $j \in \{\text{Mexico, Canada}\}$ as a measure of land route distance. We describe how we compute land route emission factors in the Online Appendix.[29]

To calculate the total emissions levels before and after IMO2023, we combine the change in container capacity ($\widehat{q}_{ijc}$), air capacity ($\widehat{q}_{ija}$), and land capacity ($\widehat{q}_{ijl}$) with 2022 trade volumes in tons transported by each respective mode. This approach allows us to incorporate mode-specific carbon efficiency (g CO_2 per ton-mile), mileage (miles), and volume (tons) into our analysis.

Manufacturing Shares. To estimate welfare changes, we assume the share of manufacturing in GDP is $\mu = 0.1$, a conservative figure, given that U.S. manufacturing's share of GDP ranged from 9.9% to 11% between 2018 and 2023 (St. Louis Fed, 2024). However, since imports of manufactured goods exceed exports, the actual consumption share could be higher. As a result, our welfare loss estimates likely represent a lower bound. Additionally, we assume the domestic share of manufacturing consumption, $\psi_{ii} = 0.65$, based on the 65% to 66% range reported for 2021 and 2022 (CPA, 2024).

5.1 Results and Discussion

For IMO2023, we present results for three scenarios, which vary in whether we allow inter-modal substitution and the adjustments in the time-sensitivity preferences ν. These results are shown in columns (1)-(3) of Table 7. In all three scenarios, ocean capacity decreases by 5.18%, ocean emissions decrease by 16.5%, and ocean freight rates increase by over 100%.[30]

The scenario depicted in (1) is the most restrictive scenario considered, as it excludes any possibility of substitution into other mode of transportation. Consequently, in (1), IMO2023 has no effect on

[29] See Online Appendix A.8.

[30] The largest drop in expenditures is 2.75%. With weight decreasing by 5.18%, this corresponds to 2.4% increase in the delivered price. Since freight rates are around 5% of delivered price, this implies a freight rate increase α calculated from $1.024 = (\alpha f + p^{FOB}\tau)/(f + p^{FOB}\tau) = (\alpha f + (1 - 0.05)f)/(f + (1 - 0.05)f) \implies \alpha = 1.05 = 105\%$. This increase is not unusual: according to data from FBX Freightos, Asia-US West Coast freight rates increased by 230% from April to July of 2021.
In practice we set $\zeta_m \forall m \in \{a, l\} = 0$ based on pass-through elasticities, reported in Online Appendix A.5, that we find to be close to zero.

the net emissions of air and land transport. These scenario is the only one in which IMO2023 leads to a reduction in combined emissions from both air and ocean transportation (-4.36%).

In scenarios (2) and (3) where substitution is allowed, net emissions rise due to two factors. First, reduced cargo capacity and higher ocean freight rates cause a 12% shift to air transport, a far more carbon-intensive mode, resulting in a 3.61% net emissions increase in scenario (2). Second, slower ocean deliveries slightly reduce the preference for ocean shipping, adding 0.03% to emissions in scenario (3), totaling 3.64%. This suggests a version of "green paradox" where regulating ocean-transport emissions increases combined emissions from all transport modes, underscoring the need for a comprehensive strategy that addresses inter-modal substitution and broader economic impacts.

The harm from IMO2023 becomes even more evident when we examine the welfare results. All three IMO2023 scenarios lead to a significant welfare losses due to reduced trade and higher consumer prices , ranging between $33.57 and $45.78 billion. These losses far outweigh any net emissions effects on welfare, which we evaluated at social marginal cost of CO_2 at $40 per ton. However, even if we apply higher marginal emission costs, as recommended by EPA (2022), with base year figures ranging from $120 to $340 per ton, the short-run welfare impact of IMO2023 will still be highly negative. To achieve welfare neutrality—where the social cost of carbon offsets the welfare loss from reduced trade and higher prices—the price of CO_2 would need to exceed $132,000 per ton in the most favorable scenario (1). This figure is several orders of magnitude higher than even the most extreme estimates of carbon's social cost. In two other scenarios such a number does not exist since IMO2023 will actually increase net emissions form transportation.

Figure 7 compares changes in total and the composition of transport related emissions as a result of IMO2023. Prior to the proposed reform, we calculate that air imported goods' share of total imports (across air, container, and land transport modes) is approximately 1.5% and yet accounts for nearly two-thirds of transport related emissions.[31] Figure 7 underscores the fact the air emissions

[31] Transport mode import shares by weight are 1.5% for air, 63.1% for container, and 35.4% by land. Emission shares depend on both the total weight and distance traveled. Transport mode import shares by ton-mile are 1.3% for air, 94.8% by container, and 3.9% by land. The decrease in land share is explained by the fact that Canada and Mexico are much closer to the United States relative to the U.S.'s maritime trading partners.

Table 7: Short-Run Scenario Summaries

Scenario		IMO2023		Speed Increase
	(1)	(2)	(3)	(4)
Inter-Modal Substitution	No	Yes	Yes	Yes
Change in Time-Senstivity Preferences?	No	No	Yes	Yes
%Δ Air Capacity	0.00	12.16	12.20	-0.72
%Δ Container Capacity	-5.18	-5.18	-5.18	0.86
%Δ Land Capacity	0.00	0.14	0.18	-0.02
%Δ Domestic Capacity	0.45	0.32	0.44	0.05
%Δ Air Expenditure	0.00	16.51	16.54	-0.92
%Δ Container Expenditure	-2.11	-1.94	-2.75	0.82
%Δ Land Expenditure	0.00	0.21	0.25	-0.03
%Δ Domestic Expenditure	0.41	0.28	0.39	0.05
%Δ Air CO_2	0.00	12.36	12.39	-0.75
%Δ Container CO_2	-15.62	-15.62	-15.62	2.49
%Δ Land CO_2	0.00	0.15	0.19	-0.02
Net Δ% CO_2	-4.36	3.61	3.63	0.21
Net Δ CO_2 (mil tons)	-0.25	0.21	0.21	0.01
Net Δ Welfare (mil USD)	-33,572.2	-35,831.1	-45,783.3	3,779.0
Δ CO_2 Welfare (mil USD)	10.1	-8.4	-8.5	-0.5
Δ Welfare (mil USD)	-33,582.3	-35,822.8	-45,774.8	3,779.5
Welfare Neutral CO_2 price (USD/ton)	132,624	n.a.	n.a.	306,027

on a per unit and total basis contribute substantially to transport-based emissions. Indeed, Figure 7 shows that the approximately 3 percent emissions share increase (allowing for inter-modal substitution) for air lines up with a comparable percentage increase in *total* net CO_2 emissions as conveyed by Table 7.

Our findings raise the question of why the IMO would propose a reform that could potentially increase combined carbon emissions from both ocean and air transportation while also lowering consumer surplus. The answer is multifaceted. Firstly, the IMO is mandated to address the specific objective of reducing emissions from ocean transportation, and IMO2023 achieves this by incentivizing ocean carriers to avoid receiving "D" and "E" ratings from their shippers. Secondly, the IMO can be seen as a self-regulating cartel, composed of representatives from carriers, shipbuilders, and

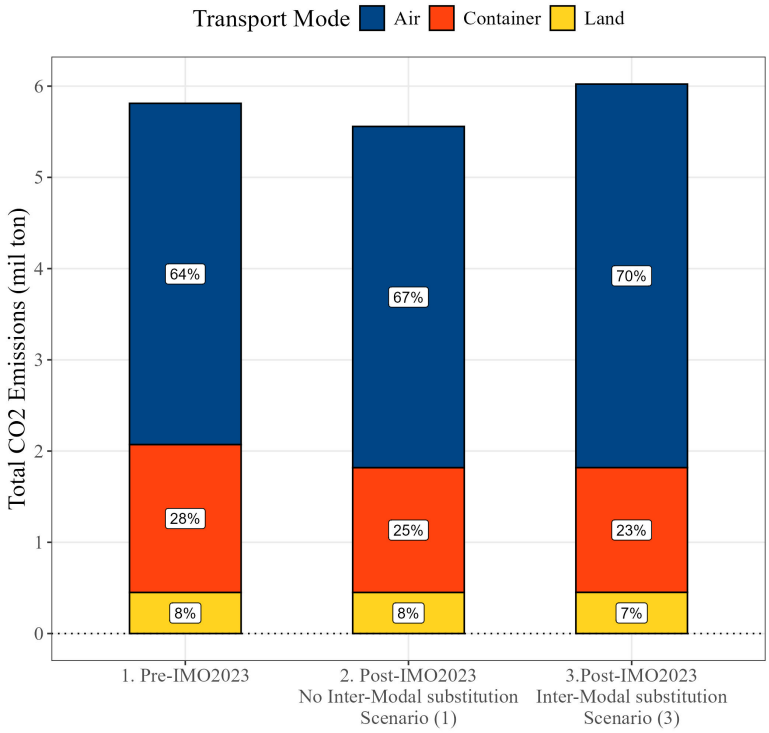


Figure 7: Short-Run Scenario Emissions Comparison

shipping-related financiers. In this sense, IMO2023 serves to satisfy other IMO-specific objectives, such as (i) boosting carriers' short-term profits and (ii) enhancing the demand for new vessels in the medium and long term.

Indeed, with the discussed above over 100% increase in freight rates and only 5.2% decrease in quantity, the implementation of IMO2023 is projected to lead to doubling of of carriers' revenue. Furthermore, shipbuilders can anticipate an increase in orders to restore shipping capacity, while bankers can expect a higher demand for shipbuilding financing. In summary, in addition to reducing carbon emissions in ocean transportation, IMO2023 also creates additional profit opportunities for all participants in the ocean-shipping industry. This situation is similar to a hypothetical scenario in which OPEC reduces oil supply, citing environmental concerns to justify their actions.

5.2 Forced speed up in the short-run?

Our inter-modal trade and emissions analysis hinges on the short-run relationship between vessel speed and capacity. Slower speeds reduce the number of round trips, cutting short-run capacity. Conversely, a modest increase in speed can expand capacity, especially since ocean container carriers typically operate near full capacity. This increase could lower freight rates and encourage substitution from air to maritime transport. Faster delivery of ocean-shipped goods would further drive this shift. Forcing vessels to speed up may have an ambiguous effect on net CO_2 emissions. While shifting from air to maritime transport reduces emissions per unit of substituted imports, speed increases result in quadratic fuel consumption rises. Nonetheless, sufficient inter-modal substitution from air to ocean transport could offset the reduced fuel efficiency in shipping.

As a self-contained thought experiment, we applied the same method previously used to analyze a 1% increase in shipping speed. The results, shown in column (4) of Table 7, are notably more favorable than any of those under short-run IMO2023 scenarios. Net emissions rise by only 0.21%, while welfare increases by $3.8 billion. However, it's important to note that these short-run findings do not extend to the long-run. In the long-run, the link between speed and additional capacity becomes less direct due to the potential entry and exit of vessels. In fact, sustained increases in speed on ocean routes without technological improvements could lead to much higher net emissions. In Section 6, we explore the long-term impacts of IMO2023 and alternative policy options.

6 Long-Run Effects of IMO2023

In the long-run, carriers' ability to deploy new containerships will eventually ease the negative impact of slow-steaming on ocean capacity. However, longer delivery times will still dampen demand for ocean transport and lead to carbon leakage into air shipping. While slow-steaming reduces bunker costs, it increases non-fuel costs per ton-mile, such as labor and financing, which rise with longer delivery times. Thus, the net effect of IMO2023 on long-run marginal costs, freight rates, and quantities depends on model parameters. We assess these effects using a similar method as in our

short-run analysis.

We begin by applying naval engineering principles and the share of fuel costs in total marginal costs to derive the formula for changes in shipping marginal costs.

Lemma 5. *In long-run equilibrium, the proportional change in the marginal cost of containerized shipping c_{jc} is a function of vessel speed s_{ij} and the aggregate containerized transportation volume on a given route q_{ij}.*

$$\widehat{c}_{jc}(\widehat{s}_{ij};\widehat{q}_{jc}) = \mu_{Fuel}\left(\left[\frac{F^{Main}\left(\frac{\widehat{s}_{ij}s_{ijt}}{s_v^{Des}}\right)^3 + F^{Aux}}{F^{Main}\left(\frac{s_{ijt}}{s_v^{Des}}\right)^3 + F^{Aux}}\right]\frac{1}{\widehat{s}_{ij}}\right) + \frac{(1-\mu_{Fuel})}{\widehat{n}_{ij}(\widehat{s}_{ij};\widehat{q}_{jc})} \tag{18}$$

where μ_{Fuel} represents the fuel's share in the marginal cost, F^{Main} and F^{Aux} are the technological parameters of the main and auxiliary engines, respectively, and n_{ij} is the number of voyages (round trips) per year.

Proof. See Online Appendix A.4. □

Next, recall from Lemma 2 that the containerized freight rate is given by: $f_{jct} = \left(\frac{\tilde{\varepsilon}}{\tilde{\varepsilon}-1}\right)c_{jct}$. Assuming $\tilde{\varepsilon}$ remains constant in the long-run, the proportional change in the containerized and non-containerized freight rate can be derived from changes in the containerized marginal cost:

$$\widehat{f}_{jc} = \widehat{c}_{jc}(\widehat{q}_{jc}) \qquad \widehat{f}_{jm} = \zeta_m\left(\widehat{c}_{jc}(\widehat{q}_{jc}) - 1\right) + 1 \quad \forall m \neq c \tag{19}$$

Using equation (10), we apply changes in the freight rates to calculate changes in the lower nest prices :

$$\widehat{p}_{ijm} = p^{\text{FOB}}_{ijmt}(\tau_{ijmt} + \widehat{f}_{ijm}f_{ijc}/p^{\text{FOB}}_{ijmt}) \tag{20}$$

Our long-run optimization procedure is similar to the short-run approach, as we again use the same optimization function described in equation (17). The key difference is that in the short-run, we treated containerized shipping as a sector with fixed capacity, considering changes in quantities ($\widehat{q}_{ijc}$) as the exogenous shock. In the long-run, instead, we consider changes in prices ($\widehat{p}_{ijc}$), driven by shifts in the marginal costs of shipping, as the exogenous shock. In the long-run optimization, we build on

our short-run results by capping air expenditures at short-run levels and ensuring container volume reductions on route ij do not exceed those seen in the short-run. The exact optimization procedure is described in Online Appendix A.6.

6.1 Results and Discussion

IMO2023 Long-Run Results. Column (1) of Table 8 shows our long-run results for IMO2023. As ship construction takes about three years (Kalouptsidi, 2014; Chokshi, 2020), it is plausible to expect that long-run effects of IMO2023 would materialize three years after implementation.

Table 8: Long-Run Scenario Summaries

Scenario	IMO2023 (1)	1% Air Tax (2)
Inter-Modal Substitution	Yes	Yes
Change in Time-Sensitivity Preferences	Yes	Yes
Δ% Air Capacity	7.61	-0.48
Δ% Container Capacity	-1.68	0.34
Δ% Land Capacity	0.90	0.00
Δ% domestic Capacity	0.15	0.00
Δ% Air Expenditure	8.47	-0.18
Δ% Container Expenditure	-2.02	0.37
Δ% Land Expenditure	0.91	0.00
Δ% Domestic Expenditure	0.12	0.00
Δ% Air CO_2	7.19	-0.38
Δ% Container CO_2	-9.52	0.37
Δ% Land CO_2	0.91	0.01
Net %Δ CO_2	2.07	-0.14
Net Δ CO_2 (mil tons)	0.12	-0.01
Net Δ Welfare (mil USD)	-13,972.6	-61.9
Δ CO_2 (mil USD)	-4.8	0.33
Δ Welfare (mil USD)	-13967.8	-223.6
Δ Tax Revenue (mil USD)	n.a.	161.4
Welfare Neutral CO_2 Price (USD/ton)	n.a.	7,650

Our findings reveal that the "green paradox"—an unintended net increase in CO_2 emissions—continues, with about a 2% annual rise in emissions. While the long-run allows for some capacity recovery, the increased marginal costs of shipping and slower delivery times still drive a shift from ocean to air transportation. This shift undermines the intended environmental benefits, as air freight is significantly more carbon-intensive, suggesting the reform may fail to meet the overall emissions reduction for the international transportation sector without further adjustments.

Second, while the long-run effect of IMO 2023 reduces welfare losses, there are still remaining losses of 14 billion USD. This indicates that, despite some improvement compared to the short-run effects, the policy continues to impose significant costs on consumers.

Slower and more expensive ocean delivery of imports could significantly harm the domestic production sector, as many imports are crucial intermediate goods. On the other hand, a shift toward domestic production might trigger scale effects that lower manufacturing prices. However, the exact impact on domestic prices remains unclear. Figure 8 examines scenarios where domestic prices change by -3% to +3%, revealing that domestic welfare is highly sensitive to these fluctuations. Even a small 1% rise in domestic prices could lead to an additional welfare loss of 18 billion USD, raising serious concerns about the broader economic consequences of IMO2023.

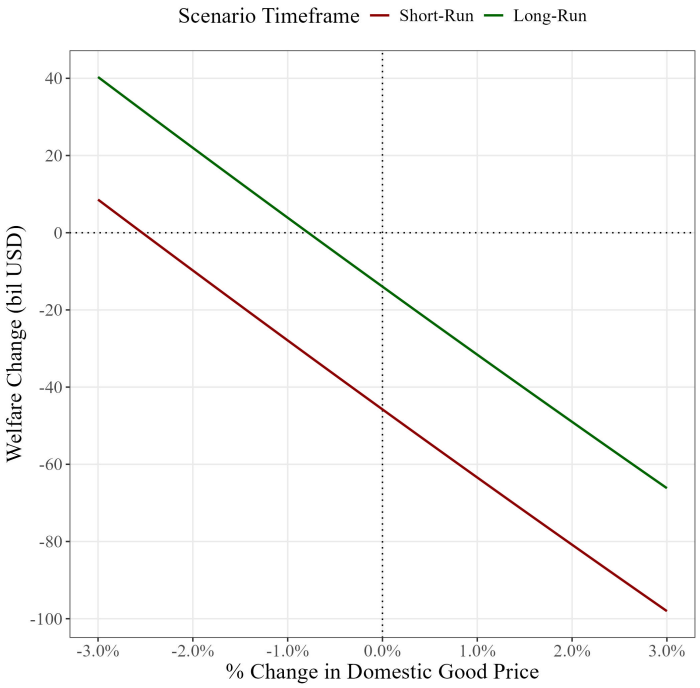


Figure 8: Domestic Price Change

As demonstrated by our findings, agencies with narrow specializations tend to prioritize their specific objectives when regulating activities. This is evident within various United Nations entities, such as the IMO, the International Civil Aviation Organization, and the United Nations Environment Programme, which develop environmental policies for sectors like ocean transportation, air travel, and production. To address inter-sectoral and environmental spillovers, the United Nations could consider restructuring its framework or broadening the mandates of these agencies.

From an environmental perspective, focusing solely on regulating ocean shipping seems misguided. The least carbon-efficient mode—air freight—should be the primary target. We propose a counterfactual where, instead of regulating ocean shipping, a 1% ad-valorem tax is imposed on air freight. Table 8 shows that this policy not only reduces air transportation emissions but also lowers overall transportation net emissions. The shift in demand from air to ocean shipping moves toward a more environmentally sustainable option, highlighting the missed opportunity in current regulations that overlook the real emissions culprit.

7 Conclusion and External Validity to Other Countries

We argue that IMO2023's implementation mechanism (read: ships slowing down) will have unintended consequences, primarily through carbon leakage into more carbon-intensive air transportation. This shift will lead to a short-term increase in combined emissions from both air and ocean transportation. In the long-run, the efficiency gains in ocean shipping will be largely offset by this leakage, resulting in a modest overall impact on emissions. Moreover, IMO2023 will negatively affect consumer surplus in both the short and long term by reducing import volumes and slowing ocean freight delivery. To mitigate these issues, we propose alternative policies such as taxing air-transported goods.

Our analysis is limited by data constraints, focusing only on transportation-related emissions and mode shifts. We do not account for production-related emissions or the potential reconfiguration of value chains, which narrows the broader applicability of our findings. A more comprehensive assessment remains beyond the scope of this study and is left for future research.

Another limitation of our paper is the focus solely on U.S. imports. This limit stems from a lack of detailed data needed to conduct similar analyses for other countries. A key question thus remains: Is the U.S. unique in its import composition, and could IMO2023's effects differ for other countries? To explore this, we use the UNCTAD Global Transport Dataset (Hoffmeister et al., 2022) to calculate the share of imports transported by air for each country, by both value and weight, as shown in Figure 9. Table A12 lists countries with a global import share above 0.5

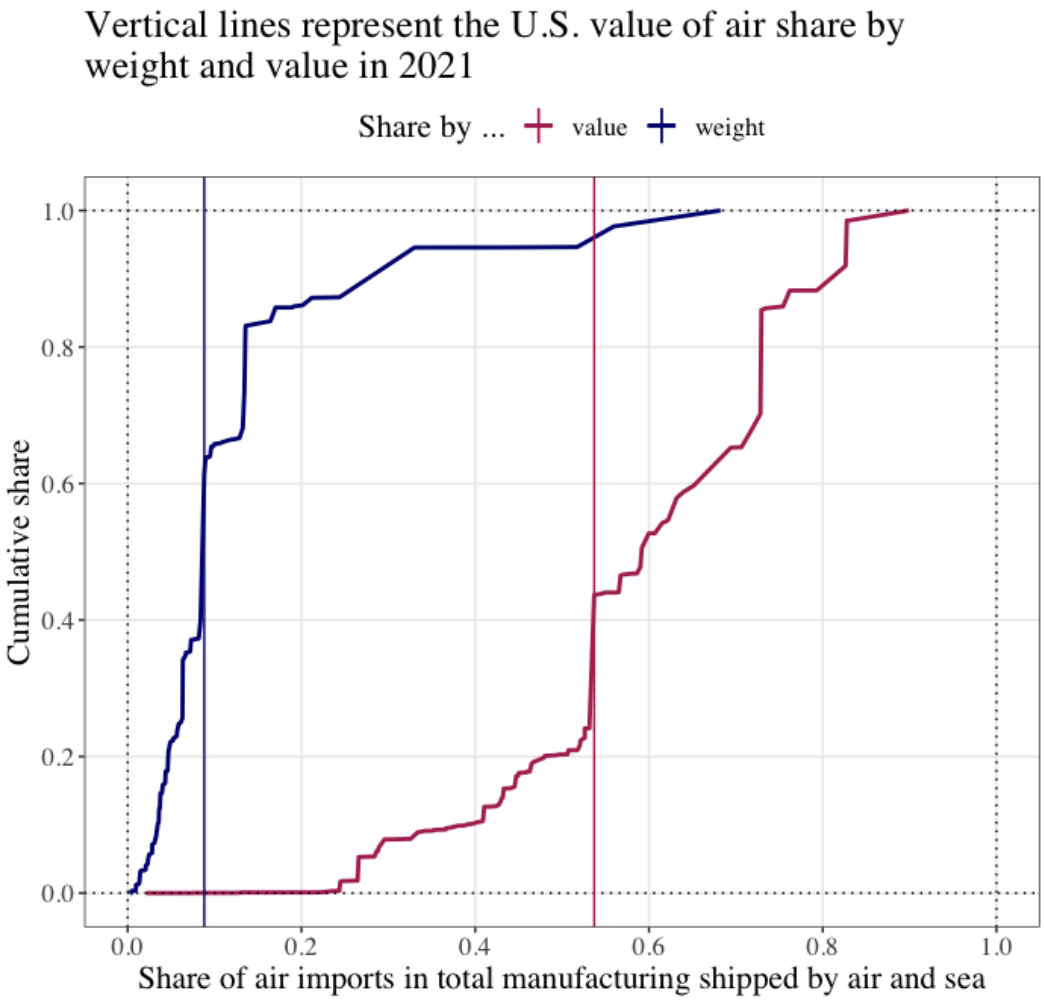


Figure 9: Air Share and Cumulative Global Share

The results show that U.S. import shares are not outliers, indicating that other countries will likely experience a similar shift from ocean to air transportation. In the short term, this suggests a "green paradox" on a global scale. Long term, taxing air freight appears to be a more effective policy for both reducing emissions and minimizing negative welfare impacts.

References

Matt Apuzzo and Sarah Hurtes. Tasked to Fight Climate Change, a Secretive U.N. Agency Does the Opposite. *The New York Times*, June 3:53–82, 2021.

Adina Ardelean and Volodymyr Lugovskyy. It pays to be big: Price discrimination in maritime shipping. *European Economic Review*, 153:104403, 2023. ISSN 0014-2921. doi: https://doi.org/10.1016/j.euroecorev.2023.104403. URL https://www.sciencedirect.com/science/article/pii/S0014292123000326.

Jose Asturias. Endogenous transportation costs. *European Economic Review*, 123:103366, 2020.

Randy Becker and Vernon Henderson. Effects of air quality regulations on polluting industries. *Journal of Political Economy*, 108(2):379–421, 2000. doi: 10.1086/262123. URL https://doi.org/10.1086/262123.

Elyakim Ben-Hakoun, Mordechai Shechter, and Yehuda Hayuth. Economic evaluation of the environmental impact of shipping from the perspective of co2 emissions. *Journal of Shipping and Trade*, 1, 2016. ISSN 2364-4575. doi: https://doi.org/10.1186/s41072-016-0011-5.

Tibor Besedeš and Antu Panini Murshidb. Experimenting with ash: The trade-effects of airspace closures in the aftermath of eyjafjallajökull. *Mimeo*, 2022.

Timothy Besley, Thiemo Fetzer, and Hannes Mueller. The welfare cost of lawlessness: Evidence from somali piracy. *Journal of the European Economic Association*, 13(2):203–239, 2015.

Bruce A. Blonigen and Wesley W. Wilson. Port Efficiency and Trade Flows. *Review of International Economics*, 16(1):21–36, February 2008.

Lucy Budd and Stephen Ison. The role of dedicated freighter aircraft in the provision of global airfreight services. *Journal of Air Transport Management*, 61:34–40, 2017. ISSN 0969-6997. doi: https://doi.org/10.1016/j.jairtraman.2016.06.003. URL https://www.sciencedirect.com/science/article/pii/S0969699715301642. Special Issue on Air Cargo: A By-Product or Success Factor?

Ching-Cheng Chao. Assessment of carbon emission costs for air cargo transportation. *Transportation Research Part D: Transport and Environment*, 33:186–195, 2014. ISSN 1361-9209. doi: https://doi.org/10.1016/j.trd.2014.06.004. URL https://www.sciencedirect.com/science/article/pii/S1361920914000698.

Niraj Chokshi. How Giant Ships Are Built. *New York Times*, 2020. URL https://www.nytimes.com/interactive/2020/06/17/business/economy/how-container-ships-are-built.html.

Brian R Copeland. Pollution content tariffs, environmental rent shifting, and the control of cross-border pollution. *Journal of International Economics*, 40(3):459–476, 1996. ISSN 0022-1996. doi: https://doi.org/10.1016/0022-1996(95)01415-2. URL https://www.sciencedirect.com/science/article/pii/0022199695014152. Symposium on Growth and International Trade: Empirical Studies.

James J Corbett, Haifeng Wang, and James J Winebrake. The effectiveness and costs of speed reductions on emissions from international shipping. *Transportation Research Part D: Transport and Environment*, 14(8):593–598, 2009.

CPA. U.s. manufacturers' share of domestic market plummets to historic low. https://prosperousamerica.org/u-s-manufacturers-share-of-domestic-market-plummets-to-historic-low/, 2024. Accessed: [insert today's date].

Anca Cristea, David Hummels, Laura Puzzello, and Misak Avetisyan. Trade and the greenhouse gas emissions from international freight transport. *Journal of Environmental Economics and Management*, 65(1):153–173, 2013. doi: 10.1016/j.jeem.2012.06.00. URL https://ideas.repec.org/a/eee/jeeman/v65y2013i1p153-173.html.

Robert Dekle, Jonathan Eaton, and Samuel Kortum. Global rebalancing with gravity: Measuring the burden of adjustment. *IMF Staff Papers*, 55(3):511–540, 2008. doi: 10.1057/imfsp.2008.17. URL https://documents1.worldbank.org/curated/en/099436104042241280/pdf/IDU0c20d2ae90046304ca009ab508217e50747bd.pdf.

Edwin Van der Werf and Corrado Di Maria. Imperfect environmental policy and polluting emissions: The green paradox and beyond. *International Review of Environmental and Resource Economics*, 6(2):153–194, 2012. ISSN 1931-1465. doi: 10.1561/101.00000050. URL http://dx.doi.org/10.1561/101.00000050.

Naihua Duan. Smearing estimate: a nonparametric retransformation method. *Journal of the American Statistical Association*, 78(383):605–610, 1983.

Joshua Elliott, Ian Foster, Samuel Kortum, Todd Munson, Fernando Pérez Cervantes, and David Weisbach. Trade and carbon taxes. *American Economic Review*, 100(2):465–69, May 2010. doi: 10.1257/aer.100.2.465. URL https://www.aeaweb.org/articles?id=10.1257/aer.100.2.465.

EPA. *Report on the Social Cost of Greenhouse Gases: Estimates Incorporating Recent Scientific Advances*. September 2022. URL https://subscriber.politicopro.com/eenews/f/eenews/?id=00000184-77c6-d07e-a5fd-f7df41f80000. This document is *Supplementary Material for the Regulatory Impact Analysis for the Supplemental Proposed Rulemaking, "Standards of Performance for New, Reconstructed, and Modified Sources and Emissions Guidelines for Existing Sources: Oil and Natural Gas Sector Climate Review."*.

Jasper Faber, Maarten 't Hoen, Marnix Koopman, Dagmar Nelissen, and Saliha Ahdour. Estimated Index Values of New Ships. Analysis of EIVs of Ships That Have Entered The Fleet Since 2009. CE Delft 15.7E50.14, 2015.

Farid Farrokhi and Ahmad Lashkaripour. Can Trade Policy Mitigate Climate Change? Mimeo, indiana university, September 2021.

Sharat Ganapati, Woan Foong Wong, and Oren Ziv. Entrepôt: Hubs, Scale, and Trade Costs. Technical report, University of Oregon, 2020.

Michael Greenstone. The impacts of environmental regulations on industrial activity: Evidence from the 1970 and 1977 clean air act amendments and the census of manufactures. *Journal of Political Economy*, 110(6): 1175–1219, 2002. doi: 10.1086/342808. URL https://doi.org/10.1086/342808.

Howard K Gruenspecht. Differentiated regulation: The case of auto emissions standards. *American Economic Review*, 72(2):328–31, 1982. URL https://EconPapers.repec.org/RePEc:aea:aecrev:v:72:y:1982:i:2:p:328-31.

Antonio Guterres. UN Secretary-General: "Making Peace with Nature is the Defining Task of the 21st century", Dec 2020. URL https://tinyurl.com/a74bwarn.

Rema Hanna. Us environmental regulation and fdi: Evidence from a panel of us-based multinational firms. *American Economic Journal: Applied Economics*, 2(3):158–89, July 2010. doi: 10.1257/app.2.3.158. URL https://www.aeaweb.org/articles?id=10.1257/app.2.3.158.

Jamie Hansen-Lewis and Michelle M Marcus. Uncharted waters: Effects of maritime emission regulation. Technical report, National Bureau of Economic Research, 2022.

Hercules E Haralambides. Gigantism in container shipping, ports and global logistics: a time-lapse into the future, 2019.

James Harrigan. Airplanes and comparative advantage. *Journal of International Economics*, 82(2):181–194, November 2010.

Onno Hoffmeister, Ronald Halim, Nicholas-Joseph Lazarou, Nour Barnat, David Cristallo, Dominik Englert, and Jan Hoffmann. Developing a global transport costs dataset for international trade. Technical Report 85, UNCTAD, 2022.

David Hummels, Volodymyr Lugovskyy, and Alexandre Skiba. The trade reducing effects of market power in international shipping. *Journal of Development Economics*, 89(1):84–97, May 2009.

David L. Hummels and Georg Schaur. Hedging price volatility using fast transport. *Journal of International Economics*, 82(1):15–25, September 2010.

David L. Hummels and Georg Schaur. Time as a Trade Barrier. *American Economic Review*, 103(7):2935–59, 2013.

David L. Hummels and Alexandre Skiba. Shipping the good apples out? an empirical confirmation of the alchian-allen conjecture. *Journal of Political Economy*, 112(6):1384–1402, 12 2004.

IMO. Third IMO GHG Study. Technical report, International Maritime Organization, 2014. URL https://www.imo.org/en/ourwork/environment/pages/greenhouse-gas-studies-2014.aspx.

IMO. Resolution MEPC.377(80): 2023 IMO Strategy on Reduction of GHG Emissions from Ships. Adopted at the 80th Session of the Marine Environment Protection Committee (MEPC), July 2023. URL https://www.imo.org/en/OurWork/Environment/Pages/GHG-Emissions.aspx. *MEPC 80/17/Add.1 Annex 15*.

International Maritime Organization. Sulphur 2020 - cutting sulphur oxide emissions, 2020. URL https://www.imo.org/en/MediaCentre/HotTopics/Pages/Sulphur-2020.aspx. Accessed: 2024-09-17.

Jota Ishikawa and Nori Tarui. Backfiring with backhaul problems. *Journal of International Economics*, 111(C): 81–98, 2018.

Mark R. Jacobsen and Arthur A. van Benthem. Vehicle scrappage and gasoline policy. *American Economic Review*, 105(3):1312–38, March 2015. doi: 10.1257/aer.20130935. URL https://www.aeaweb.org/articles?id=10.1257/aer.20130935.

Myrto Kalouptsidi. Time to build and fluctuations in bulk shipping. *American Economic Review*, 104(2):564–608, February 2014. doi: 10.1257/aer.104.2.564. URL https://www.aeaweb.org/articles?id=10.1257/aer.104.2.564.

David Kershaw. Hapag-lloyd preparing for turbulent 2023, Nov 2022. URL https://www.heavyliftpfi.com/sectors/hapag-lloyd-preparing-for-turbulent-2023/21719.article.

Valentina Keys. Bimco cii clause finally released: Does it make any sense of cii?, Dec 2022a. URL https://www.wfw.com/articles/bimco-cii-clause-finally-released-does-it-make-any-sense-of-cii/.

Valentina Keys. The cii conundrum – will it sink or swim?, Dec 2022b. URL https://www.wfw.com/articles/the-cii-conundrum-will-it-sink-or-swim/.

Amit Khandelwal. The Long and Short (of) Quality Ladders. *Review of Economic Studies*, 77(4):1450–1476, 2010.

Brian G. Kinyua. Shipping's decarbonization outlook for 2023. *Maritime Executive*, January 2023. URL https://maritime-executive.com/editorials/shipping-s-decarbonization-outlook-for-2023.

Samuel Kortum and David A. Weisbach. Optimal Unilateral Carbon Policy. Technical report, 2021.

Ahmad Lashkaripour and Volodymyr Lugovskyy. Profits, Scale Economies, and the Gains from Trade and Industrial Policy. *American Economic Review*, 113(10):2759–2808, October 2023. doi: 10.1257/aer.20210419. URL https://www.aeaweb.org/articles?id=10.1257/aer.20210419.

Andrei A. Levchenko, Logan T. Lewis, and Linda L. Tesar. The "collapse in quality" hypothesis. *American Economic Review*, 101(3):293–97, May 2011.

Jasmina Ovcina Mandra. Maersk ceo: We will need 5-15% more capacity to meet imo 2023, Aug 2022. URL https://www.offshore-energy.biz/maersk-ceo-we-will-need-5-15-more-capacity-to-meet-imo-2023/.

James R. Markusen. International externalities and optimal tax structures. *Journal of International Economics*, 5 (1):15–29, 1975. ISSN 0022-1996. doi: https://doi.org/10.1016/0022-1996(75)90025-2. URL https://www.sciencedirect.com/science/article/pii/0022199675900252.

Gabriela Mundaca, Jon Strand, and Ian R. Young. Carbon pricing of international transport fuels: Impacts on carbon emissions and trade activity. *Journal of Environmental Economics and Management*, 110:102517, 2021. ISSN 0095-0696. doi: https://doi.org/10.1016/j.jeem.2021.102517. URL https://www.sciencedirect.com/science/article/pii/S009506962100084X.

Hellenic Shipping News. Shipping giant Maersk&x2019;s shift into air freight is undermining its green ambitions | Hellenic Shipping News Worldwide — hellenicshippingnews.com. 2021.

William Nordhaus. Climate clubs: Overcoming free-riding in international climate policy. *American Economic Review*, 105(4):1339–70, April 2015. doi: 10.1257/aer.15000001. URL https://www.aeaweb.org/articles?id=10.1257/aer.15000001.

Ian Parry, Mr Dirk Heine, Kelley Kizzier, and Tristan Smith. *Carbon taxation for international maritime fuels: Assessing the options*. International Monetary Fund, 2018.

Arthur Pigou. *The Economics of Welfare*. Macmillan, London, 1920.

Mohit Sanguri. How to use main engine performance curve for economical fuel consumption on ships, 2023. URL https://www.marineinsight.com/main-engine/how-to-use-main-engine-performance-curve-for-economical-fuel-consumption-on-ships/. Accessed: 2024-09-17.

Joseph S Shapiro. Trade costs, co2, and the environment. *American Economic Journal: Economic Policy*, 8(4): 220–54, 2016.

Joseph S Shapiro. The Environmental Bias of Trade Policy*. *The Quarterly Journal of Economics*, 136(2):831–886, 12 2020. ISSN 0033-5533. doi: 10.1093/qje/qjaa042. URL https://doi.org/10.1093/qje/qjaa042.

Powell Slaughter. Next year's carbon emissions standards could further complicate ocean shipping, May 2022. URL https://www.furnituretoday.com/supply-chain/next-years-carbon-emissions-standards-could-further-complicate-ocean-shipping/.

St. Louis Fed. Value added by private industries: Manufacturing as a percentage of gdp in massachusetts (vapgdpma). https://fred.stlouisfed.org/series/VAPGDPMA, 2024. Accessed: [insert today's date].

Martin Stopford. page 669–673. Routledge, 2009.

Mark Szakonyi. Slow steaming, congestion to blunt container capacity injections: Zim, Aug 2021. URL https://www.joc.com/maritime-news/container-lines/zim-integrated-shipping-services/slow-steaming-congestion-blunt-2023-container-capacity-injections-zim_20210818.html.

Shinsuke Tanaka, Kensuke Teshima, and Eric Verhoogen. North-south displacement effects of environmental regulation: The case of battery recycling. *American Economic Review: Insights*, 4(3):271–88, September 2022. doi: 10.1257/aeri.20210201. URL https://www.aeaweb.org/articles?id=10.1257/aeri.20210201.

Jens Thomsen. Congestion keeps growing—427 vessels idle in major container ports. *Shippingwatch.com*, 2021. URL https://shippingwatch.com/carriers/Container/article13312358.ece.

UNCTAD. UNCTAD Assessment of the Impact of the IMO Short-Term GHG Reduction Measure on States. Tech. report, United Nations Conference on Trade and Development, 2021.

USCG. Office of commercial vessel compliance (cg-cvc): International convention for the prevention of pollution by ships - marpol 73/78, 2022. URL https://www.dco.uscg.mil/Our-Organization/Assistant-Commandant-for-Prevention-Policy-CG-5P/Inspections-Compliance-CG-5PC-/Commercial-Vessel-Compliance/Domestic-Compliance-Division/MARPOL/.

Tony R. Walker, Olubukola Adebambo, Monica C. Del Aguila Feijoo, Elias Elhaimer, Tahazzud Hossain, Stuart Johnston Edwards, Courtney E. Morrison, Jessica Romo, Nameeta Sharma, Stephanie Taylor, and Sanam Zomorodi. Chapter 27 - environmental effects of marine transportation. In Charles Sheppard, editor, *World Seas: An Environmental Evaluation (Second Edition)*, pages 505–530. Academic Press, second edition edition, 2019. ISBN 978-0-12-805052-1. doi: https://doi.org/10.1016/B978-0-12-805052-1.00030-9. URL https://www.sciencedirect.com/science/article/pii/B9780128050521000309.

Hulda Winnes, Linda Styhre, and Erik Fridell. Reducing ghg emissions from ships in port areas. *Research in Transportation Business & Management*, 17:73–82, 2015.

Woan Foong Wong. The Round Trip Effect: Endogenous Transport Costs and International Trade. Technical report, University of Oregon, 2020.

Woan Foong Wong and Simon Fuchs. Multimodal transport networks. 2022.

Tianle Yuan, Hua Song, Robert Wood, Chenxi Wang, Lazaros Oreopoulos, Steven E Platnick, Sophia von Hippel, Kerry Meyer, Siobhan Light, and Eric Wilcox. Global reduction in ship-tracks from sulfur regulations for shipping fuel. *Science advances*, 8(29):eabn7988, 2022.

A Online Appendix—For Online Publication

A.1 Detailed Data Description

In this section, we present two types of the data description: (i) a table, which provides name of all datasets, their key variables, purposes of using these dataset, and Section(s) of the paper where a particular dataset is used; and (ii) a more detailed description of some datasets used in the paper.

Table A1: Summary of Datasets Used in the Paper and Online Appendix

Name of the Dataset	Key Variables	Purpose of Using the Dataset	Section
IMO2023 Regulations	Required emissions per vessel size (Dead Weight Tonnage, Dwt)	To compare actual emissions per vessel with those required by IMO2023 regulations	Section 2, Online Appendix A.3.6
World Fleet Register (WFR), Clarksons PLC	Dead Weight Tonnage (Dwt) and other technical characteristics of individual containerized vessels	To analyze current emissions by vessel size and calculate the required speed adjustments to meet IMO2023 standards	Section 2, Online Appendix A.2,A.3
THETIS-MRV, by the European Maritime Safety Agency (EMSA)	Measured annual carbon emissions and distance traveled per vessel	To obtain actual per-vessel emissions data for comparison with the benchmark emissions set by IMO2023	Section 2, Online Appendix A.2,A.3
Shipping Intelligence Network (SIN), Clarksons PLC	Idle capacity data for vessels	To demonstrate that containerized shipping operates at full capacity	Section 2, Online Appendix A.2,A.3
Automatic Identification System (AIS), Marine Cadastre	AIS tracking data for container ships serving U.S. ports	To estimate port time and analyze its relationship with traffic levels	Section 2, Online Appendix A.3.7
U.S. Census Imports Data	Freight rates, quantities, and product prices by mode of transportation	To estimate demand- and supply-side parameters for the model	Section 3, Online Appendix A.2,A.3,A.5,A.9
Panjiva	Bill of lading data	To identify U.S.-bound container ships and calculate vessel operational speeds	Section 2, Online Appendix A.2,A.3
BlueWater Reporting	Ship rotation data	To identify container ship routes and calculate speed reduction required by IMO2023	Section 2, Online Appendix A.2,A.3 A.7
Domestic and International Segment T100 Traffic Data	Air cargo capacity utilization	To assess excess capacity in air transportation and its impact on air freight rates	Section 3
UNCTAD Global Transport Dataset	Air and ocean share of traded goods	To provide back-of-the-envelope global assessment of IMO2023.	Section 7
Global Rural-Urban Mapping Project, Version 1 (GRUMPv1): Settlement Points	Gridded global population estimates for the entire world	To create population-weighted coordinates for U.S. Custom Districts	Online Appendix A.9

Technical characteristics of each vessel (vessel size, engine type, eco-equipment, design fuel consumption, etc.), which will allow us to predict speed changes to meet the required IMO2023 CII. These data come from the *World Fleet Register* (WFR), maintained by Clarksons PLC—the world's leading shipbroker—and include all major commercial vessels.

Actual (observed) fuel consumption, distance traveled, and carbon emissions provided by THETIS-MRV (alternatively THETIS), an online, port state control/inspection database maintained by the European Maritime Safety Agency (EMSA). It was launched in August 2017 in an effort to support new owner reporting requirements pursuant to Regulation (EU) 2015/757 on Monitoring, Reporting, and Verification of CO_2 from marine transport. Regulation 2015/757 requires the owners to report carbon emissions per transport work for

all vessels that (i) are larger than 5,000 gross tonnage (GT); and (ii) make at least one call to an EU territory port subsequent to January 1st, 2018. THETIS-MRV makes provisions for third party monitoring and verification of a ship owner's reported carbon emissions. THETIS-MRV's data on owner-reported technical efficiency is publicly available, and features annual emissions reports from 2018-2020.

There are roughly 15,000 unique IMO number-vessels in the THETIS-MRV database across 2018-2020. Our preferred efficiency rating is the Energy Efficiency Design Index (EEDI), which measures grams of CO_2 generated per ton-nautical mile. THETIS also records vessel Estimated Index Values (EIV). EIV ratings, relative to EEDI ratings, are: (i) better thought of as vessel design efficiency metric versus as a fuel efficiency rating; (ii) less data-intensive to calculate due to making simplifying assumptions about vessel operation; and (iii) tend to slightly overestimate EEDI ratings (Faber et al., 2015).

Data on container carriers, their service rotations and capacities on all routes worldwide between 2012 and 2020, provided by BlueWater Reporting. These data will allow us to determine the capacity and speed of ocean transportation on importing routes to the U.S.

Matching different datasets. We link each vessel found in the THETIS-MRV registry back to the Clarksons' World Fleet Registry through the vessel's unique IMO number. The Clarksons-THETIS merge of the global containerized ocean fleet results in a match of 39.7% by count and 54.1% by capacity. The match is less than 100% because under THETIS carbon emissions were measured only from the vessels entering European ports, while Clarksons contains information about the entire global fleet. For comparison, the corresponding numbers for the bulk fleet are 42.3% and 38.5%, respectively. BlueWater Reporting contains all containerized maritime routes, which allows us to match (using the IMO number) each containership present in either Clarksons or THETIS with its route in a given month.

A.2 Route Construction and Carrier Count

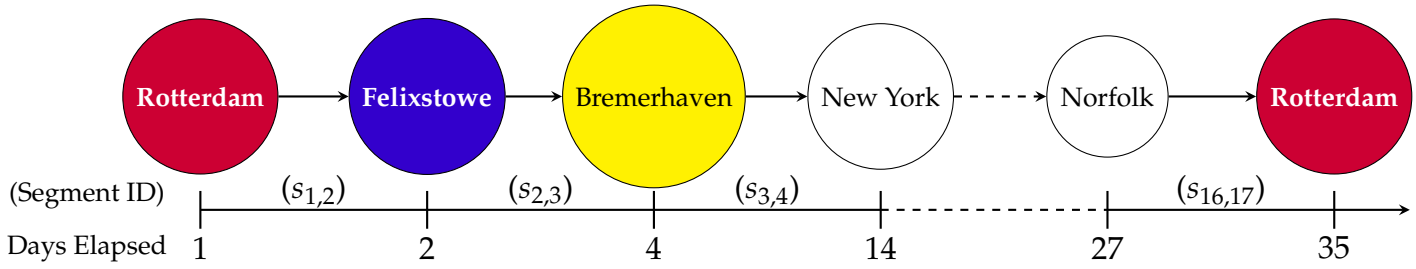


Figure A1: Container Rotation Example

Notes:: Port nodes are colored by country. Port to port pairs are identified by Segment ID $s_{i,j}$, where i, j indexes port stops (from stop i to stop j). Ports can be visited more than once whereas stop numbers are unique, e.g. Rotterdam is the 1st and 17th stop in the rotation. Finally, port stops between New York and Norfolk are excluded for illustrative simplicity. Carriers APL, CMA CGM, Hyundai, and Maersk Line service this rotation at various points throughout 2013.

A typical observation within BlueWater Reporting's historical rotation data lists the origin and destination port pair alongside the rotation that the pair belongs to. The rotation is a semi-colon separated string in the following form: "PortX 1 ; PortY 2" where a port name is followed by the number of days that have elapsed since the start of the rotation. In this way, a rotation can be thought of a sequence of port-to-port segments with a corresponding travel time given by the difference in the number of days elapsed. Additionally, each rotation lists the names of servicing carriers.

A BlueWater route is thus a sub-sequence of a larger rotation. The listed origin-destination pair, which serve as the endpoints of the route, *are not necessarily the endpoints* of a rotation. Moreover, BlueWater does not necessarily breakout all segments of a rotation. To put the problem in concrete terms, consider the example provided by Figure A1. BlueWater lists Rotterdam (origin port) to New York (destination port) as a route with the larger rotation. This rotation is serviced by four (4) carriers: APL, CMA CGM, Hyundai, and Maersk Line. Rotterdam (NL) to New York includes intermediate stops in Felixstowe (GB) and Bremerhaven (DE). Thus, there are at least four (4) carriers that serve New York from: the Netherlands; the United Kingdom; and Germany. However, BlueWater might *explicitly* report the four (4) carriers between the Netherlands and New York but not report the four (4) carriers between the United Kingdom and New York.

We clean our BlueWater rotation data to determine the number of carriers that service Country-U.S. Customs District *routes* according to the following steps:

1. **Identify all unique ports across all rotations**. Port names are not necessarily unique. After cleaning, our sample includes 462 ports.

2. **Geo-code ports**. For each of the 462 ports, we determine the longitude/latitude coordinates.

3. **Map ports into countries and/or U.S. Customs Districts**. Based on the port name and coordinates, we then map ports to countries. If the port is American, we further map the port into the relevant U.S. Customs District. We map Panjiva port to a given Custom District based on the minimum (great-circle) distance between a port and a Custom District's average longitude/latitude coordinates. Please refer to Online Appendix A.9 for additional information on how we construct average Custom District coordinates.

4. **Determine each rotation's total distance and time**. Since each rotation can be broken down into port-to-port pairs, we compute the sea distance traveled for each port pair.[32] Interestingly enough, at 3,769 unique pairs, the total number of unique port-to-port pairs is small relative to the theoretical maximum: $\frac{3{,}769}{462\times(461)/2} \approx 3.5\%$. Port pair travel time is based on the difference in total time elapsed. For example, Figure A1's segment $s_{3,4}$ implies a travel time of 10 days. Moreover, we calculate a sea distance of 4,230 miles (compared to the 4,000 mile estimate from SP PortWorld.

A.3 From ship speed to route capacity changes

The following details how we process our shipping micro data to determine both changes in speed, capacity and CO_2 per ton mile post IMO2023 reforms on a per route basis (e.g. U.S. Customs District-country or ij) relative to our 2022 base year.[33]

A.3.1 Identify which ships service which routes for 2019

We look to our BlueWater Reporting and Panjiva datasets to determine which container ships serviced route ij in 2019. Both our datasets report individual vessel IMO numbers (i.e. unique vessel identifiers) and report which port/country a vessel originated from and the U.S. port of arrival in 2019. Our first step is to identify unique ships across both datasets. All told, we have $n = 1,826$ unique vessels: 985 vessels are common to both datasets whereas 226 (615) ships are unique to BlueWater Reporting (Panjiva). Denote this list of unique (U.S. 2019 bound) vessels as `imo_vessel_list19`.

[32] Besley et al. (2015) provides details about how to use GIS data and R to compute shortest paths over sea between port pairs.

[33] Our shipping micro data do not extend to 2022, the year which serves as our baseline for our counterfactual analysis. We use 2019 data for this paper because it represents the most recent year of complete data that we have access to.

A.3.2 Determine vessel speed for 2019

Once we have `imo_vessel_list19`, our next step is to determine the average speed for each vessel: we use BlueWater Reporting and THETIS-MRV to determine average vessel speed.

1. BlueWater Reporting data provides a rotation schedule for a given ship where we can see each port visited and transit duration between ports measured in days. BlueWater specifies the origin-destination ports within a rotation (e.g. London (UK) to Boston (US)): we use these end points to define a ship's trip. Using Dijkstra's algorithm as adapted by Besley et al. (2015), we compute the sea-distance between each port-to-port segment. Next, we sum up distance and transit time across all segments so that we know total (sea) travel distance and time. Average transit speed is thus total (sea) distance divided by total travel time. We use a vessels assigned weekly capacity as weights when computing average speed. In this way, we are able to compute 1,138 average vessel speeds.

2. THETIS data indirectly allows us to compute average vessel speed. THETIS reports a ship's annual CO_2 emissions; THETIS also reports a ship's CO_2 output while at berthing at port. We subtract a ship's berthing emissions from its annual emissions to determine its annual emissions while at moving at sea. THETIS lists a ship's average CO_2 emissions per nautical mile; combining average emissions per nautical mile with total emissions from movement at sea allows us to recover a ship's total mileage at sea. Converting this sea-mileage figure, we then use THETIS's reported annual hours at sea to come up with an average mile-per-hour estimate for each ship. In this way, we compute an additional 338 average speed estimates for ships in `imo_vessel_list19`.

BlueWater and THETIS thus allow us to estimate average traveling speed for 1,470 out of 1,826 ships (or 81 % of our sample). Figure A2 charts the relationship between vessel size and average speed. BlueWater and THETIS derived speeds share comparable distributions and both datasets convey a positive relationship between vessel size[34] and average speed. However, the relationship between vessel size and average speed holds relatively modest explanatory power, with a simple regression line's $R^2 = 0.18$. For this reason, we impute a median speed of 16.245 mph to all remaining 356 ships. Our imputed speed is close to Clarksons' SIN 2019 average containership speed (for all containerships) of 14.36 knots or 16.53 mph.

[34] Vessel size in Figure A2 comes from Clarksons WFR.

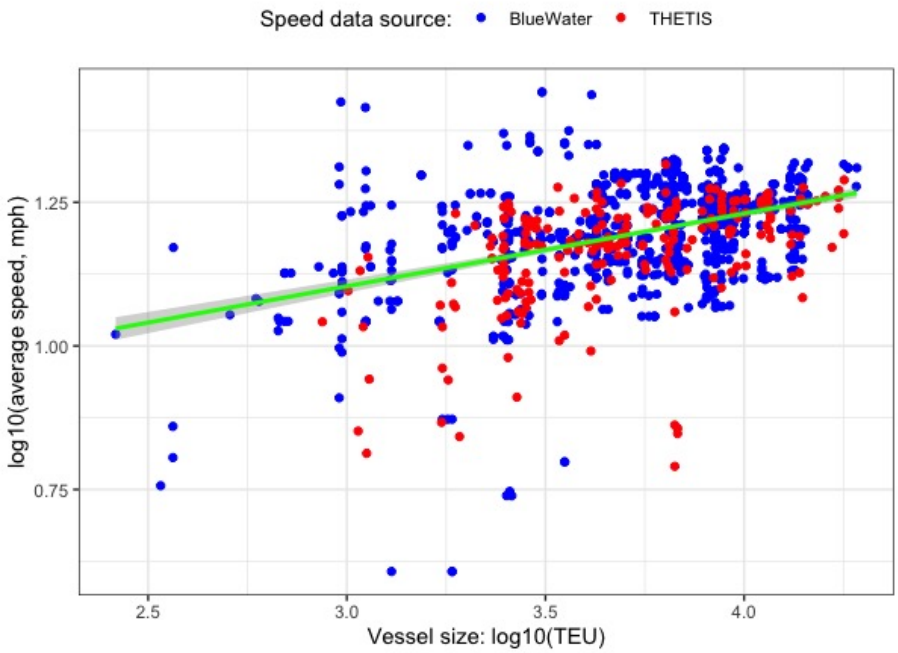


Figure A2: Ship size vs operational speed

Notes: Green line is the regression line that comes from regressing (log) average vessel speed on (log) vessel size. The slope coefficient is positive and statistically different from zero, namely $\beta = 0.127$ 95% CI[0.112, 0.141], and the model's $R^2 = 0.18$.

A.3.3 Approximating vessel technical characteristics related to fuel consumption

We use data from Clarksons WFR, which allows us to match vessel v's size expressed in deadweight tonnage, Dwt_v, with engines' main and auxiliary fuel consumption and design speed (s_v^{Des}). We use the following specification:

$$\log(x_v) = \alpha_1 + \alpha_2 \log(Dwt_v) + \epsilon_v,$$

where x_v sequentially represents F_v^{Main}, F_v^{Aux}, and s_v^{Des}. We apply a Seemingly Unrelated Regression (SUR) estimator to simultaneously estimate all coefficients. Table A2 presents the results.

Table A2: Vessel Size as a predictor of Fuel Consumption and Speed

Dependent variable:	$\log(F_v^{\text{Main}})$	$\log(F_v^{\text{Aux}})$	$\log(s_v^{\text{Des}})$
(Intercept)	-4.861^{***}	-5.087^{***}	6.068^{***}
	(0.057)	(0.194)	(0.512)
$\log(Dwt_v)$	0.884^{***}	0.632^{***}	0.308^{***}
	(0.005)	(0.018)	(0.047)
R^2	0.867	0.484	0.430
Num. obs.	4046	329	370
Duan Smear	1.041	1.080	1.034

Notes: $^{***}p < 0.01$; $^{**}p < 0.05$; $^{*}p < 0.1$

Filling in missing vessel size. There are 297 vessels that are in `imo_vessel_list19` that do not appear in Clarksons' WFR. We use Vessel Tracking to look up each of these 297 vessels and retrieve vessel information as available: this website lists vessel TEU capacity rather than Dwt capacity. Our use of Vessel Tracking returns 220 vessels that $TEU_v > 0$. We use data from Clarksons' WFR to translate TEUs into Dwt via a simple linear model. Table A3 presents this simple "conversion" model:

Table A3: Mapping TEU to Dwt

Dependent variable:	Dwt_v
(Intercept)	5703.848***
	(146.036)
TEU	10.637***
	(0.026)
R^2	0.982
Adj. R^2	0.982
Num. obs.	3189
RMSE	6101.592

Notes: $^{***}p < 0.01$; $^{**}p < 0.05$; $^{*}p < 0.1$

For the remaining 297-220=77 vessels, we impute our data's median Dwt of 66,940 tons. Once we have Dwt information for all vessels, we impute any missing information on engines' main and auxiliary fuel consumption and design speed; we default to Clarksons' WFR if those characteristics are present there.

A.3.4 Imputing vessel CII

We use pooled THETIS data across the 2018-2021 reporting periods and vessel size (e.g. Dwt) from Clarksons' WFR to compute vessel CII scores, $CII^{obs}_{v,t}$. We estimate two regression models—one model that simply uses vessel size measured in Dwt to predict $CII^{obs}_{v,t}$ and another model that controls for year effects—and report our results in Table A4:[35]

[35] We trim one vessel-year from the merged THETIS (Year)-Clarksons dataset because it is an outlier: $CII^{obs}_{v,t} > 1000$.

Table A4: Imputing CII

Dependent variable: $\log(CII^{obs}_{v,t})$		
	(1)	(2)
(Intercept)	7.650^{***}	7.671^{***}
	(0.023)	(0.023)
log(Dwt)	-0.490^{***}	-0.490^{***}
	(0.002)	(0.002)
2019		-0.027^{***}
		(0.006)
2020		-0.043^{***}
		(0.006)
2021		-0.015^{**}
		(0.006)
R^2	0.879	0.880
Adj. R^2	0.879	0.880
BIC	-4584.829	-4617.023
Num. obs.	7190	7190
Duan Smear	1.015	1.015

Notes: $^{***}p < 0.01$; $^{**}p < 0.05$; $^{*}p < 0.1$

We use the regression model specification of column (2) within Table A4 to impute CII scores for vessels in `imo_vessel_list19` that don't appear in THETIS.

A.3.5 Vessel data source summary

Table A5 summarizes where/what combination of sources/methods our vessel data from when we construct `imo_vessel_list19`: Figure A3 depicts the empirical cumulative distribution function (ECDF) for vessel capacity per data series/source. Broadly speaking, all data series have similar capacity distributions.

Table A5: Vessel data sources for `imo_vessel_list19`

Speed	Dwt	Main Engine (F^{Main})	Auxiliary Engine (F^{Aux})	Design Speed (s_v^{Des})	$CII_{v,t}^{obs}$	Count
BW	Clarksons	Clarksons	(II)	(II)	(III)	379
BW	Clarksons	Clarksons	(II)	(II)	THETIS	374
THETIS	Clarksons	Clarksons	(II)	(II)	THETIS	176
(I)	Clarksons	Clarksons	(II)	(II)	(III)	149
(I)	Vessel Track	(II)	(II)	(II)	(III)	130
BW	Clarksons	(II)	(II)	(II)	(III)	109
THETIS	Vessel Track	(II)	(II)	(II)	(III)	68
BW	Clarksons	(II)	(II)	(II)	THETIS	62
BW	Clarksons	Clarksons	(II)	Clarksons	(III)	59
BW	Clarksons	Clarksons	Clarksons	(II)	(III)	58
THETIS	(I)	(II)	(II)	(II)	(III)	43
(I)	(I)	(II)	(II)	(II)	(III)	33
BW	Clarksons	Clarksons	(II)	Clarksons	THETIS	24
THETIS	Clarksons	(II)	(II)	(II)	THETIS	23
BW	Vessel Track	(II)	(II)	(II)	(III)	22
BW	Clarksons	Clarksons	Clarksons	(II)	THETIS	19
(I)	Clarksons	Clarksons	Clarksons	(II)	(III)	17
(I)	Clarksons	Clarksons	(II)	Clarksons	(III)	17
BW	Clarksons	(II)	(II)	Clarksons	(III)	16
BW	Clarksons	(II)	(II)	Clarksons	THETIS	15
THETIS	Clarksons	Clarksons	(II)	Clarksons	THETIS	11
THETIS	Clarksons	Clarksons	Clarksons	(II)	THETIS	8
(I)	Clarksons	(II)	(II)	(II)	(III)	7
(I)	Clarksons	(II)	(II)	Clarksons	(III)	3
THETIS	Clarksons	(II)	(II)	Clarksons	THETIS	3
BW	(I)	(II)	(II)	(II)	(III)	1

Notes: Imputation Method (I): We use the median speed and Dwt across our pooled BlueWater (BW) and THETIS data to impute missing values.
Imputation Method (II): We use a seemingly unrelated regression (SUR) estimator, built on Clarksons WFR data, to impute vessel characteristics as function of vessel Dwt.
Imputation Method (III): We estimate a simple regression model where observed carbon intensity is a function of vessel Dwt and use this model to impute carbon intensity.

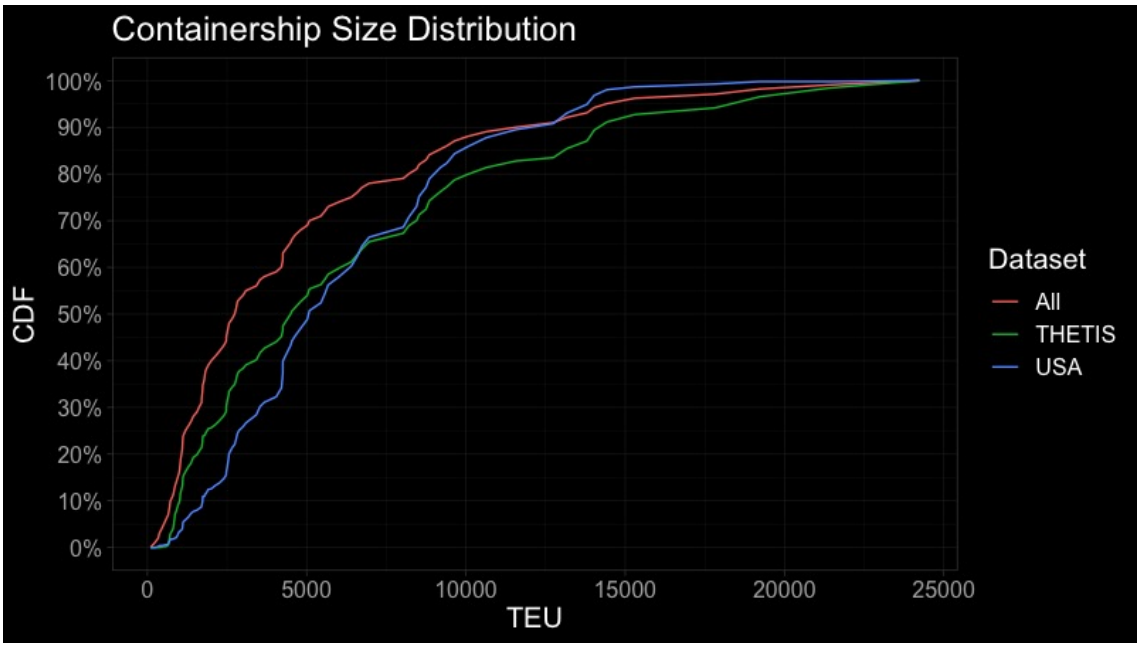


Figure A3: Size Comparison

A.3.6 Modeling IMO Speed Adjustments

Now that `imo_vessel_list19` is complete with respect to technical characteristics, speed, and carbon intensity, we use Corbett et al. (2009)'s formula, equation (A21), to model the relationship between a vessel's speed and fuel consumption (subject to vessel characteristics):

$$F_{ijv}(s_v) = \left[F_v^{\text{Main}}\left(\frac{s_v}{s_v^{\text{Des}}}\right)^3 + F_v^{\text{Aux}}\right]\frac{d_{ij}}{24 s_v},, \tag{A21}$$

where d_{ij} is the route distance. Suppose that $s_v^{\text{IMO}} = \rho_v s_v$ is the speed that will ensure that v is compliant with IMO2023 carbon intensity standards, namely that ships are no more than 107% over the required emissions line (as to score a letter "C" or better):

$$CII_{v,t}^{req}(Z_t) = \left[1984 \times (Dwt_v)^{-0.489}\right](1 - Z_t) \implies \frac{CII_{v,t}^{obs}}{CII_{v,t}^{req}} \times \leq 107\%$$

where $(1 - Z_t) = 0.95$ for $t = 2023$.[36]
For each ship in `imo_vessel_list19`, we use Brent's method to find the speed adjustment factor ρ_v^* that solves:

$$\rho_v^*(Z_t) \in \arg\min H(\rho_v) \equiv \left(1 - \left(\frac{\overline{CII}_v^{obs}}{\overline{CII}_v^{req}(Z_t)} - 1.07\right) - \frac{F_v\left(s_{1v}^{\text{IMO}}(\rho_v(Z_t))\right)}{F_v(s_{1v})}\right)^2 \tag{A22}$$

We set $\rho_v^* = 1$ for IMO2023 compliant ships (e.g. "C" grade or better). Figure 2 in the text visualizes our results

[36] See MEPC.338(76) for the Z_t schedule over the next several years: starting in 2023, $Z_t = 5\%$ with an additional 2 percentage points added each year after 2023.

for ρ_v^* across all `imo_vessel_list19` containerships. In the event that we calculate $\rho_v > 1$ for ships that are currently rated as "D" or "E", this means that these ships will be unable to reduce their speed enough to comply with IMO standards. In this case of IMO2023 standards, the number of these ships is less than five (5). When we take our speed estimates over to our capacity adjustment calculations, we drop these ships from our capacity-analysis.

A.3.7 Estimating time in port

The number of trips that a ship can make in a year partially depends on how much time is spent in port. We follow a similar strategy to Wong and Fuchs (2022) in using Automatic Identification System (AIS) provided by MarineCadastre.gov. These AIS data are the result of collaborative efforts between the U.S. Bureau of Ocean Energy Management (OECM), the National Oceanic and Atmospheric Administration (NOAA), and the U.S. Coast Guard Navigation Center. In total, these AIS data cover nearly all vessel movements off the U.S. coastline reported in one minute intervals for every day since January 1st, 2015 (with more limited coverage stretching back to 2009). Downloading all of these data would require several terabytes (TB) of computer storage.

Awash in a sea of data, we make a number of judgement calls to make these vessel tracking data more amenable to our purposes.

- **First**, we limit our attention to January 2019 vessel tracking.
- **Second**, using Clarksons's WFR data on all containership MMSI (Maritime Mobile Service Identity) numbers—a unique number that identifies individual ships—we are able to filter out all non-containerships from the MarineCadastre data. This filtering step leaves us with 3,105,5772 AIS readings for 610 containerships.
- **Third**, our AIS data include COLREGS (International Regulations for Preventing Collisions at Sea) vessel navigational codes. These codes describe what the vessel is doing when it transmits the AIS signal. We limit our attention to AIS readings with navigation status codes "0" (Under way using its engine),"1" (anchored), and "5" (Moored or tied to another object to limit free movement): these codes describe the two statuses we are interesting, namely whether the vessel is moving or docked. Filtering on these navigation status codes brings our sample down to 3,090,059 AIS signals and keeps at 610 vessels. As a sanity check, we use the AIS's SOG (speed over ground, knots per hour) data to confirm that ship is relatively stationary while a "1" of "5" code is active.
- **Fourth**, we re-code our three reminaing COLREGS status to capture whether or not a containership is moving. For each containership in our MarineCadastre, we identify runs in our data between moving/non-moving (e.g. if we code moving status as "M" and non-moving status as "N", then we look for the first time an uninterrupted sequence of "M"'s is broken by an "N"). Once we the terminal points of non-moving code sequence, we find the corresponding (terminal) time stamps and so compute the duration of the vessel's stationary episode.
- **Fifth**, we use Panjiva U.S. 2019 bill of lading data to identify all U.S container ports and geo-reference all container port. For every vessel's stationary period, we take the average longitude/latitude position of the vessel and use that point to find the closest Panijvia U.S. container port. If the vessel's non-stationary location is more than 50 miles away from the port, we exclude this stationary episode from our analysis.
- Figure A4 gives an example of what our clean AIS data look like for a given ship, the COSCO Excellence (IMO: 9472189), and its various stops in the early part of January 2019. In particular, we see that

COSCO Excellence first stopped outside of Savannah, GA (denoted by "A" across panels) before entering and unloading that port (denoted by "B") before repeating the waiting and unloading stages in Charleston, SC ("C" and "D" respectively) before heading west out to sea. In context, we consider the sum of the times in periods "A" and "B" ("C" and "D") as COSCO Excellence's port time period for Savannah, GA (Charleston, SC). The port time for COSCO Excellence is roughly 164 (43) hours for Savannah,GA (Charleston, SC).

- **Sixth**, we compute a rough measure of port-day traffic in a manner similar to Wong and Fuchs (2022). For each ship in our sample, we calculate the share of a given day that a ship spends in a port and multiply this share by the deadweight (Dwt) tonnage capacity of the ship. For example, if a 78,300 Dwt container ship were docked outside of Oakland, CA from January 2nd 2:00AM to January 4th 6:00PM, we would add $22/24 \times 78,300 = 71,790$ tons on January 2nd to Oakland's traffic measure and $24/24 \times 78,300 = 78,300$tons on January 3rd and $6/24 \times 78,300 = 19,575$ tons on January 4th. We then sum over each port-day to compute our traffic measure, port traffic$_{pd}$.

- **Seventh**, we aggregate port locations together such that if our data have two or more ports within a 20 miles radius of each other, we group them together. In this way, we jointly consider the ports of Los Angeles/Long Beach, Seattle/Tacoma, New York/Newark, etc.

- **Eighth**, armed with 50 ports, 524 container ships, and 1,236 port visits, we estimate a set of simple fixed effect regression models that predict a vessel's port time as function of its deadweight capacity. Our unit of analysis here is a ship v on day d visiting port p: the dependent variable is (log) days in port for ship v on day d visiting port p. Each column of Table A6 indicates that increases in vessel size are associated with higher expected port times: even in the most stringent specification in column (3), a 10% increase in vessel time raises expected dwell time by 2.8%. Column (3)'s $p \times d$ fixed effects encompass port and day specific influences on a vessel's expected dwell time, such as *port congestion*. We use the port fixed effects from column (2) to create the dwell time map presented by Figure A5. With the exception of Wilmington DE, containerships entering any major U.S. container port experience between 20 to 80% less dwell time conditional on vessel size relative to Los Angeles/Long Beach.

Table A6: Port Time as a Function of Vessel Size

	Dependent variable: log (port time$_{vpd}$)		
	(1)	(2)	(3)
(Intercept)	1.418***		
	(0.506)		
log(Dwt$_{vd}$)	0.181***	0.111*	0.284***
	(0.046)	(0.064)	(0.079)
Num. obs.	1236	1236	1236
R^2 (full model)	0.013	0.350	0.700
R^2 (proj model)		0.004	0.032
Adj. R^2 (full model)	0.012	0.305	0.421
Adj. R^2 (proj model)		0.003	0.030
FE: port (p)		✓	
FE: day (d)		✓	
FE: port $\times$ day ($p \times d$)			✓

Notes: $^{***}p < 0.01$; $^{**}p < 0.05$; $^{*}p < 0.1$

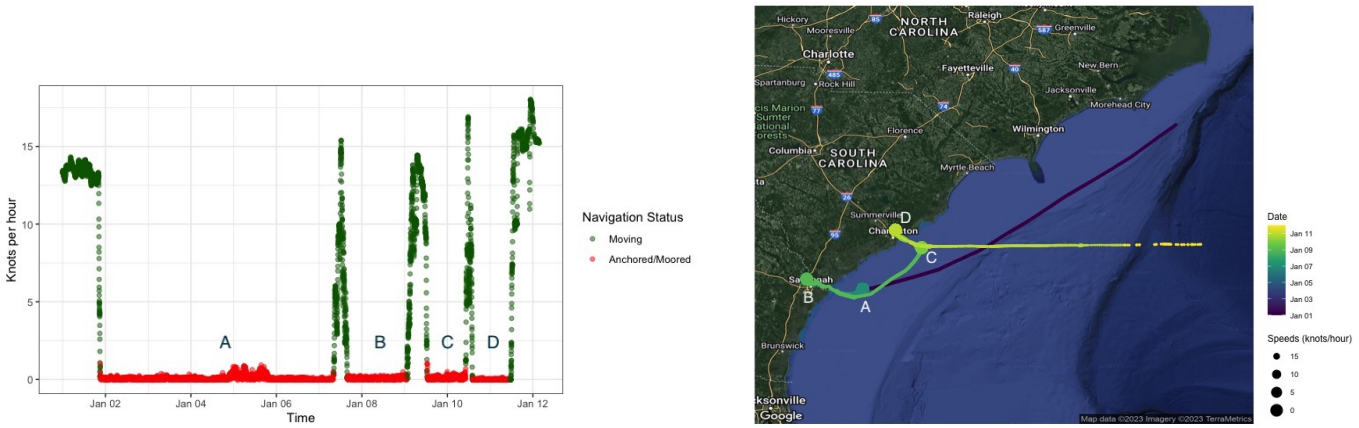
We also (partially) replicate Wong and Fuchs (2022) regression analysis connecting port traffic to port service times. As a quick outline of differences Wong and Fuchs (2022): (i) use data on a wider selection of ships from June 2015 to December 2021; (ii) focus on a ship's *dwell time*, or the time a vessel "spends being moored at a pier and has zero speed" (e.g. periods in "B" and "D" in our Figure A4); and (iii) calculate port traffic over moving multi-day/week averages. These differences notwithstanding, we find similar a qualitatively similar port time elasticity with respect to traffic: a 10% increase in traffic today is associated with a 1.97% increase in a ship's vessel time in port (e.g. column 4) compared to Wong and Fuchs (2022) preferred elasticity of 1.3%.

Table A7: Port time as function of port traffic?

	Dependent variable: log (port time$_{vpd}$)			
	(1)	(2)	(3)	(4)
(Intercept)	0.437*			
	(0.256)			
log(port traffic$_{pd}$)	0.205***	0.234***	0.210***	0.197***
	(0.017)	(0.068)	(0.051)	(0.058)
Num. obs.	1236	1236	1236	1236
R^2 (full model)	0.101	0.317	0.382	0.764
R^2 (proj model)		0.070	0.053	0.057
Adj. R^2 (full model)	0.100	0.288	0.339	0.542
Adj. R^2 (proj model)		0.069	0.052	0.055
FE: port (p)		✓	✓	✓
FE: day (d)			✓	✓
FE: vessel (v)				✓

Notes: $^{***}p < 0.01$; $^{**}p < 0.05$; $^{*}p < 0.1$

- **Ninth**, our Table A6 regression specifications' relatively low *adjusted* R^2's suggest that considerable explanatory power is left unaccounted for. For this reason, we choose to adopt a uniform measure of port time via a two step weighted average: (i) we average January 2019 port time per container port in our sample using our definition of port traffic$_{pdv}$ as weights; and, (ii) we use Panjiva bill of lading data to compute 2019 annual traffic per port which we use to identify the top 20 ports by TEU volume. We then use average these twenty container port times (from the previous step) while using their annual TEU volumes as weights. In this way, we compute an aggregated port time measure of **2.53 days (60.8 hours)**.



(a) Vessel speed vs movement status (b) Vessel path

Figure A4: COSCO Excellence (IMO: 9472189) trip to Savannah, GA and Charleston, SC



Figure A5: 2019 estimated port time for top 20 U.S. container ports

Notes: Ports are scaled in size to proportion of their annual TEU volume. Port time's are weighted by the container's port traffic$_{pd}$ flows across January 2019.

A.3.8 Filling in missing values on route distance, time, and carbon intensity

In order to analyze changes in vessel speed and their impact on route time, carbon intensity, and carbon output, it is first necessary to establish a route's distance, time, and carbon intensity. Directly observed data mapping ships to routes and route times can be used to assign vessel-capacity weighted averages of ship speed and carbon intensity per route. However, the available Census trade data on containerized imports includes U.S. Customs District-country pairs that are not covered by our vessel microdata. To address this issue, we have developed a route characteristics imputation approach, which we describe in detail below.

(a) **Direct measurements**

(a) Our analysis of trade routes involves the use of **direct measurements of distance and time, obtained from the BlueWater platform.** Priority is given to distance and travel time data for a specific route ij that is either directly reported by BlueWater (e.g., the total days in transit between ports), or that can be inferred from BlueWater data (e.g., port-to-port distance calculations converted into route distances). In total, we have access to 615 U.S. Customs District-country pairs from the BlueWater platform, along with associated IMO vessel numbers.

(b) **Direct route measures of carbon intensity:** We use our BlueWater vessel/route data to compute a vessel-capacity weighted average of carbon intensity $CII_{v,t}^{obs}$ per route.

(b) **Indirect measurements**

(a) **Indirect distance measurements**. For all remaining routes, we utilize indirect distance measurements to calculate the sea distance between BlueWater U.S. Customs District-country pairs. Specifically, we use the coordinates of a country's largest city, obtained from CEPII's GeoDist database, and average coordinates of a U.S. Customs District as our distance endpoints.[37] By incorporating these distance estimates, we are able to analyze an additional 2,684 routes in our analysis.

(b) **Indirect travel speed and distance estimates**. Once we have obtained sea distance measurements for each ij route, we utilize our non-BlueWater Panjiva vessels and their voyages' U.S. Customs District-country endpoints to calculate travel time, assuming a constant moving speed that we have previously computed. It is important to note a subtle but significant distinction between the Panjiva bill of lading data and the BlueWater data. Specifically, the bill of lading information pertains to the city/port (and therefore, the country) of origin, the port of lading (and therefore, the country), and the U.S. port of unlading (and therefore, the U.S. Customs District). We treat the country of origin as j, but we compute the distance for route ij as a shipment-weighted average distance and shipping speed between U.S. Customs District i and the port of lading in country j'. Formally, our indirect measure of $x \in$ distance, speed for ships v serving route ij and using country j' as a stop is:

$$\overline{x}_{ij}^{\text{indirect}} = \frac{\sum_{v \in ij} x_{v,ij'j} \times ship_{v,ij'j}}{\sum_{v \in ij} ship_{v,ij'j}} \tag{A23}$$

where $ship_{v,ij'j}$ is v's total shipment volume to ij using j' measured in TEUs. Using (A23), we compute average travel distance and speed for 364 additional routes.

[37] To the extent that a country's largest city is not on the country's coastline (or even if the country is landlocked), our shortest sea-path code still takes the shortest path to the nearest point of coastline and then draws a straight line (as the crow flies) over land.

(c) **Indirect estimates travel time, vessel size, and carbon efficiency**. At this stage, we have route characteristics for only 979 out of 3,295 routes. To impute the remaining route characteristics, we have devised the following strategy. If route ij is missing vessel data, we first utilize ship-capacity size weighted average speed/Dwt/$\overline{CII}_v^{obs}$ values based on country j. In the event that we are unable to compute a country average, we then attempt to compute a U.S. Customs District i average. Finally, if we cannot calculate an average using either i or j, we compute an average over all geographies.

(c) **Other measurements**. As a measure of air route distance, we compute the great circle distance between the average coordinates of the U.S. Customs Districts and the country coordinates from CEPII's GeoDist database.

Table A8 presents a summary of our maritime route-level characteristics and their respective sources. Notably, the median summary statistics pertaining to route travel speed and carbon intensity are relatively consistent across our different data sources and imputation methods, providing reassurance of the validity and reliability of our findings.

Table A8: Data Sources for Route Characteristics

Route Sources		Count	(I) values				
Travel time	Other characteristics		Dwt	Distance (miles)	Travel time (days)	Speed (mph)	CII^{obs}
BW	Route Average	611	62000	7958	22.4	15.8	10.2
Country Average	Country Average	2243	77411	7826	22.2	15.0	9.1
Country Average	Route Average	205	77859	6702	19.8	14.6	8.9
District Average	District Average	31	90804	7855	21.3	16.1	7.7
Panjiva	Country Average	11	92766	7202	23.9	17.0	8.2
Panjiva	Route Average	194	78962	6903	20.3	15.5	9.0

A.3.9 Modeling capacity adjustments caused by speed adjustments

The number of annual round trips that a ship v can make during the year on route ij is equal to:

$$\text{Round Trips} : n_{ij,v} = \frac{A}{2(d_{ij}/(24s_{ij,v}) + \text{port time})}$$

A is the number of sailing days in the year and $d_{ij}/(24s_{ij,v})$ is the average route time of vessel v moving distance d_{ij} at average speed $s_{ij,v}$ (mph).[38] A vessel's reduced capacity on route

A.4 Theoretical Proofs

A.4.1 Proof of Lemma 1.

Proof. From equation (7),

$$Q_{ijt} = \left(\frac{P_{ijt}}{P_{it}}\right)^{-\sigma} Q_{it},$$

[38] We assume that vessels are active for A =340 days out of the year to reflect off-hire periods or when statutory maintenance, dry docking, etc. This is the number used by Haralambides (2019). The choice of A arguably is inconsequential since when we calculate the ratio of round trips, we are assuming that the number of sailing days per year is unaffected.

where P_{ijt} is the district-origin specific price index as defined by equation (7), and $P_{it} \equiv \left(P_{iit}^{1-\sigma} + \sum_j P_{ijt}^{1-\sigma}\right)^{\frac{1}{1-\sigma}}$ and $Q_{it} \equiv \left(Q_{iit}^{\frac{\sigma-1}{\sigma}} + \sum_j Q_{ijt}^{\frac{\sigma-1}{\sigma}}\right)^{\frac{\sigma}{\sigma-1}}$ are the district i's price and quantity indexes.

The demand for the imports by i from country j by mode m is then given by

$$q_{ijmt} = \nu_{ijmt}^{\varepsilon}\left(\frac{p_{ijmt}}{P_{ijt}}\right)^{-\varepsilon}\left(\frac{P_{ijt}}{P_{it}}\right)^{-\sigma}Q_{it} = \nu_{ijmt}^{\varepsilon}p_{ijmt}^{-\sigma}\left(\frac{p_{ijmt}}{P_{ijt}}\right)^{\sigma-\varepsilon}P_{it}^{\sigma}Q_{it} = \nu_{ijmt}^{\varepsilon\frac{\sigma-1}{\varepsilon-1}}p_{ijmt}^{-\sigma}\lambda_{ijmt}^{\left(1-\frac{\sigma-1}{\varepsilon-1}\right)}P_{it}^{\sigma}Q_{it}, \tag{A24}$$

where λ_{ijmt} is the share of a given mode of transportation in total imports by i from j:

$$\lambda_{ijmt} = \nu_{ijmt}^{\varepsilon}\left(\frac{p_{ijmt}}{P_{ijt}}\right)^{1-\varepsilon} = \frac{p_{ijmt}q_{ijmt}}{\sum_{m\in M_{ijt}}p_{ijmt}q_{ijmt}}$$

For the last step in equation (A24), note that

$$\nu_{ijmt}^{\varepsilon}\left(\frac{p_{ijmt}}{P_{ijt}}\right)^{\sigma-\varepsilon} = \nu_{ijmt}^{\varepsilon}\left(\left(\frac{p_{ijmt}}{P_{ijt}}\right)^{1-\varepsilon}\right)^{\frac{\sigma-\varepsilon}{1-\varepsilon}} = \nu_{ijmt}^{\varepsilon\frac{\sigma-1}{\varepsilon-1}}\left(\nu_{ijmt}^{\varepsilon}\left(\frac{p_{ijmt}}{P_{ijt}}\right)^{1-\varepsilon}\right)^{1-\frac{\sigma-1}{\varepsilon-1}} = \nu_{ijmt}^{\varepsilon\frac{\sigma-1}{\varepsilon-1}}\lambda_{ijmt}^{1-\frac{\sigma-1}{\varepsilon-1}}$$

□

A.4.2 Proof of Lemma 2

Proof. Let us focus on the containerized ocean transportation on a given route ij. From equation (10), we can express the freight rate as

$$f_{ijct} = p_{ijct} - p_{ijct}^{\text{FOB}}\tau_{ijct}. \tag{A25}$$

where index c denotes the containerized ocean shipping. We can then find the delivered price also from the demand function expressed by equation (12):

$$p_{ijct} = q_{ijct}^{-\frac{1}{\varepsilon}}\nu_{ijmt}P_{ijt}^{1-\frac{\sigma}{\varepsilon}}P_{it}^{\frac{\sigma}{\varepsilon}}Q_{it}^{\frac{1}{\varepsilon}} = (q_{ijct}^{l} + \sum_{k\neq l}q_{ijct}^{k})^{-\frac{1}{\varepsilon}}\nu_{ijct}\left(\nu_{ijct}^{\varepsilon}p_{ijct}^{1-\varepsilon} + \sum_{m\neq c}\nu_{ijmt}^{\varepsilon}p_{ijmt}^{1-\varepsilon}\right)^{\frac{1}{1-\varepsilon}(1-\frac{\sigma}{\varepsilon})}P_{it}^{\frac{\sigma}{\varepsilon}}Q_{it}^{\frac{1}{\varepsilon}}, \tag{A26}$$

where q_{ijct}^{l} is the containerized quantity delivered on ij by carrier l and $\sum_{k\neq l}q_{ijct}^{k}$ is the quantity delivered by all other carriers indexed by r on the same route, such that $q_{ijct} = q_{ijct}^{l} + \sum_{k\neq l}q_{ijct}^{k}$.

Next, we apply Implicit differentiation to get the derivative of p_{ijct} with respect to q_{ijct}^{l}:

$$\frac{\partial p_{ijct}}{\partial q^l_{ijct}} = \frac{-\frac{1}{\varepsilon}\left(q^l_{ijct}+\sum_{k\neq l} q^k_{ijmt}\right)^{-\frac{1}{\varepsilon}-1} \nu_{ijct}\cdot\left(\nu^\varepsilon_{ijct}p^{1-\varepsilon}_{ijct}+\sum_{m\neq c}\nu^\varepsilon_{ijmt}p^{1-\varepsilon}_{ijmt}\right)^{\frac{1}{1-\varepsilon}(1-\frac{\sigma}{\varepsilon})} P_{it}{}^{\frac{\sigma}{\varepsilon}} Q^{\frac{1}{\varepsilon}}_{it}}{1-\left(q^l_{ijct}+\sum_{k\neq l} q^k_{ijmt}\right)^{-\frac{1}{\varepsilon}}\cdot\nu_{ijct}\cdot P_{it}{}^{\frac{\sigma}{\varepsilon}} Q^{\frac{1}{\varepsilon}}_{it}\cdot\frac{1-\frac{\sigma}{\varepsilon}}{1-\varepsilon}\left(\nu^\varepsilon_{ijct}p^{1-\varepsilon}_{ijct}+\sum_{m\neq c}\nu^\varepsilon_{ijmt}p^{1-\varepsilon}_{ijmt}\right)^{\frac{1}{1-\varepsilon}(1-\frac{\sigma}{\varepsilon})-1}\cdot\nu^\varepsilon_{ijct}(1-\varepsilon)p^{-\varepsilon}_{ijct}}$$

$$= \frac{-\frac{1}{\varepsilon}\left(q^l_{ijct}+\sum_k q^k_{ijct}\right)^{-1} p_{ijct}}{1-p_{ijct}\frac{1-\frac{\sigma}{\varepsilon}}{1-\varepsilon}\left(\nu^\varepsilon_{ijct}p^{1-\varepsilon}_{ijct}+\sum_{m\neq c}\nu^\varepsilon_{ijmt}p^{1-\varepsilon}_{ijmt}\right)^{-1}\cdot\nu^\varepsilon_{ijct}(1-\varepsilon)p^{-\varepsilon}_{ijct}}$$

$$= \frac{-\frac{1}{\varepsilon}\left(q^l_{ijct}+\sum_k q^k_{ijct}\right)^{-1} p_{ijct}}{1-(1-\frac{\sigma}{\varepsilon})\left(1+\sum_{m\neq c}\frac{\nu^\varepsilon_{ijmt}p^{1-\varepsilon}_{ijmt}}{\nu^\varepsilon_{ijct}p^{1-\varepsilon}_{ijct}}\right)^{-1}} = -\frac{1}{\varepsilon}\left(q^l_{ijct}+\sum_{k\neq l} q^k_{ijct}\right)^{-1} p_{ijct}\frac{\left(1+\sum_{m\neq c}\frac{\nu^\varepsilon_{ijmt}p^{1-\varepsilon}_{ijmt}}{\nu^\varepsilon_{ijct}p^{1-\varepsilon}_{ijct}}\right)}{\left(\frac{\sigma}{\varepsilon}+\sum_{m\neq c}\frac{\nu^\varepsilon_{ijmt}p^{1-\varepsilon}_{ijmt}}{\nu^\varepsilon_{ijct}p^{1-\varepsilon}_{ijct}}\right)}$$

Next, we use this result to calculate the corresponding elasticity:

$$\frac{\partial p_{ijct}}{\partial q^l_{ijct}}\frac{q^l_{ijct}}{p_{ijct}} = -\frac{1}{\varepsilon}\left(q^l_{ijct}+\sum_{k\neq l} q^k_{ijct}\right)^{-1} q^l_{ijct}\left(1-(1-\frac{\sigma}{\varepsilon})\lambda_{ijct}\right)^{-1} \tag{A27}$$

Recall that carriers compete à la Cournot, with all carriers having the same symmetric marginal cost and no differentiation or loyalty incentives in ocean transportation. As a result, in equilibrium, all carriers will charge the same freight rate, f_{ijct}. This freight rate will be a function of the aggregate equilibrium quantity on that route, q_{ijct}. Specifically, from the inverse demand function (A26) combined with equation (A25), we can express the freight rate as:

$$f_{ijct} = (q^l_{ijct}+\sum_{k\neq l} q^k_{ijmt})^{-\frac{1}{\varepsilon}}\nu_{ijct}\left(\nu^\varepsilon_{ijct}p^{1-\varepsilon}_{ijct}+\sum_{m\neq c}\nu^\varepsilon_{ijmt}p^{1-\varepsilon}_{ijmt}\right)^{\frac{1}{1-\varepsilon}(1-\frac{\sigma}{\varepsilon})} P_{it}{}^{\frac{\sigma}{\varepsilon}} Q^{\frac{1}{\varepsilon}}_{it} - p^{FOB}_{ijct}\tau_{ijct}, \tag{A28}$$

where q^l_{ijct} is the quantity supplied on ij by carrier l. Using the above equation we can calculate the freight rate elasticity with respect to q^l_{ijct} :

$$\frac{\partial f_{ijct}}{\partial q^l_{ijct}} = \frac{-\frac{1}{\varepsilon}\left(q^l_{ijct}+\sum_{k\neq l} q^k_{ijct}\right)^{-\frac{1}{\varepsilon}-1}\cdot\nu_{ijct}\cdot\left(\nu^\varepsilon_{ijct}p^{1-\varepsilon}_{ijct}+\sum_{m\neq c}\nu^\varepsilon_{ijmt}p^{1-\varepsilon}_{ijmt}\right)^{\frac{1}{1-\varepsilon}(1-\frac{\sigma}{\varepsilon})}\cdot P_{it}{}^{\frac{\sigma}{\varepsilon}} Q^{\frac{1}{\varepsilon}}_{it}}{1-\left(q^l_{ijct}+\sum_{k\neq l} q^l_{ijct}\right)^{-\frac{1}{\varepsilon}}\cdot\nu_{ijct}\cdot P_{it}{}^{\frac{\sigma}{\varepsilon}} Q^{\frac{1}{\varepsilon}}_{it}\cdot\frac{1-\frac{\sigma}{\varepsilon}}{1-\varepsilon}\left(\nu^\varepsilon_{ijct}p^{1-\varepsilon}_{ijct}+\sum_{m\neq c}\nu^\varepsilon_{ijmt}p^{1-\varepsilon}_{ijmt}\right)^{\frac{1}{1-\varepsilon}(1-\frac{\sigma}{\varepsilon})-1}\cdot\nu^\varepsilon_{ijct}(1-\varepsilon)p^{-\varepsilon}_{ijct}},$$

from which we calculate the corresponding elasticity:

$$\frac{\partial f_{ijct}}{\partial q^l_{ijct}}\frac{q^l_{ijct}}{f_{ijct}} = -\frac{1}{\varepsilon}\frac{(f_{ijct}+p^{FOB}_{ijct}\tau_{ij})}{f_{ijct}}\left(q^l_{ijct}+\sum_{k\neq l} q^k_{ijct}\right)^{-1} q^l_{ijct}\left(1-(1-\frac{\sigma}{\varepsilon})\lambda_{ijct}\right)^{-1} \tag{A29}$$

Next, we are turning to the profit function by carrier l serving the route ij :

$$\pi^l_{ijct} = q^l_{ijct}(f_{ijct}-c_{ijct}) - C \qquad \forall l = 1,2,...,n_{ij}$$

Consider that the route ij is served by n_{ijct} carriers. Then, the $n_{ijct} \times 1$ vector of the first order conditions is:

$$\frac{\partial \pi_{ij}^{l}}{\partial q_{ijct}^{l}} = f_{ijct}\left(1 + \frac{\partial f_{ijct}}{\partial q_{ijct}^{l}} \frac{q_{ijct}^{l}}{f_{ijct}}\right) - c_{ijct} = 0$$

Next, we substitute for $\frac{\partial f_{ijct}}{\partial q_{ijct}^{l}} \frac{q_{ijct}^{l}}{f_{ijct}}$ with the result in equation (A29):

$$f_{ij}\left(1 - \frac{1}{\varepsilon}\frac{(f_{ijct} + p_{ijct}^{FOB}\tau_{ij})}{f_{ijct}}\left(q_{ijct}^{l} + \sum_{k \neq l} q_{ijct}^{k}\right)^{-1} q_{ijct}^{l}\left(1 - (1 - \frac{\sigma}{\varepsilon})\lambda_{ijct}\right)^{-1}\right) - c_{ij} = 0$$

In the symmetric equilibrium $n_{ijct} q_{ijct}^{l} = q_{ijct}$ which allows us to modify it as

$$f_{ij}\left(1 - \frac{1}{\varepsilon}\frac{(f_{ijct} + p_{ijct}^{FOB}\tau_{ij})}{f_{ijct}}\frac{1}{n_{ijct}}\left(1 - (1 - \frac{\sigma}{\varepsilon})\lambda_{ijct}\right)^{-1}\right) - c_{ij} = 0$$

from which

$$f_{ijct} = c_{ij} + f_{ijct}\frac{1}{\varepsilon}\frac{(f_{ijct} + p_{ijct}^{FOB}\tau_{ij})}{f_{ijct}}\frac{1}{n_{ijct}}\left(1 - (1 - \frac{\sigma}{\varepsilon})\lambda_{ijct}\right)^{-1}$$

$$f_{ijct} n_{ijct}\varepsilon\left(1 - (1 - \frac{\sigma}{\varepsilon})\lambda_{ijct}\right) = c_{ij} n_{ijct}\varepsilon\left(1 - (1 - \frac{\sigma}{\varepsilon})\lambda_{ijct}\right) + (f_{ijct} + p_{ijct}^{FOB}\tau_{ij})$$

$$f_{ijct}\left[n_{ijct}\varepsilon\left(1 - (1 - \frac{\sigma}{\varepsilon})\lambda_{ijct}\right) - 1\right] = c_{ij}\left[n_{ijct}\varepsilon\left(1 - (1 - \frac{\sigma}{\varepsilon})\lambda_{ijct}\right) - 1\right] + c_{ij} + p_{ijct}^{FOB}\tau_{ij}$$

from which

$$f_{ijct} = c_{ij} + \frac{c_{ij} + p_{ijct}^{FOB}\tau_{ij}}{n_{ijct}\varepsilon\left(1 - \lambda_{ijct}(1 - \frac{\sigma}{\varepsilon})\right) - 1} = c_{ij} + \frac{c_{ij} + p_{ijct}^{FOB}\tau_{ij}}{n_{ijct}\zeta - 1} \tag{A30}$$

where

$$\zeta = \varepsilon\left(1 - \lambda_{ijct}(1 - \frac{\sigma}{\varepsilon})\right).$$

Next, we need to show that this equation can be transformed into equation (13) in Lemma 2, which allows for a better expositional connection to other classes of models. For brevity in this derivation, we will remove all the subscripts, and we will start with the last part of equation (A30).

$$\begin{aligned} f &= c + \frac{c + p^{FOB}\tau}{n\zeta - 1} = \frac{n\zeta c - c}{n\zeta - 1} + \frac{c + p^{FOB}\tau}{n\zeta - 1} \\ &= \frac{n\zeta c}{n\zeta - 1} - \frac{c}{n\zeta - 1} + \frac{c}{n\zeta - 1} + \frac{p^{FOB}\tau}{n\zeta - 1} = \frac{n\zeta c}{n\zeta - 1} + \frac{p^{FOB}\tau}{n\zeta - 1} \end{aligned}$$

from which:

$$f(n\zeta - 1) = n\zeta c + p^{FOB}\tau \quad \Longrightarrow \quad n\zeta c = n\zeta f - f - p^{FOB}\tau,$$

from which:

$$f = \frac{n\zeta f}{n\zeta f - f - p^{FOB}\tau}c = \frac{\frac{n\zeta f}{f + p^{FOB}\tau}}{\frac{n\zeta f - f - p^{FOB}\tau}{f + p^{FOB}\tau}}c$$
$$= \frac{n\zeta\left(\frac{f}{f + p^{FOB}\tau}\right)}{n\zeta\left(\frac{f}{f + p^{FOB}\tau}\right) - 1}c = \frac{n\zeta\left(\frac{f}{p}\right)}{n\zeta\left(\frac{f}{p}\right) - 1}c = \frac{\tilde{\epsilon}}{\tilde{\epsilon} - 1}c$$

where

$$\tilde{\epsilon} \equiv n\frac{f}{p}\zeta = n\frac{f}{p}\varepsilon\left(1 - \lambda_{ijct}(1 - \frac{\sigma}{\varepsilon})\right)$$

□

A.4.3 Proof of Lemma 3

Proof. For our utility function (7), the ratio of the indirect utility functions can be expressed as

$$\widehat{W}_i = \frac{\left[P_{iiT}^{1-\sigma} + \sum_{j\neq i} P_{ijT}^{1-\sigma}\right]^{\frac{-\mu}{1-\sigma}}}{\left[P_{iit}^{1-\sigma} + \sum_{j\neq i} P_{ijt}^{1-\sigma}\right]^{\frac{-\mu}{1-\sigma}}}.$$

Using the "exact hat algebra", as in Dekle et al. (2008), we can re-write it as

$$\widehat{W}_i = \left[\psi_{iit}\widehat{P}_{ii}^{1-\sigma} + \sum_{j\neq i}\psi_{ijt}\widehat{P}_{ij}^{1-\sigma}\right]^{\frac{-\mu}{1-\sigma}}.$$

where $\widehat{X}$ represents the proportional change in X between period t and the new time period T, i.e., $\widehat{X} = \frac{X_T}{X_t}$. The terms ψ_{iit} and ψ_{ijt} denote the shares of products iit and ijt in the consumption of manufacturing goods in region i. □

A.4.4 Proof of Lemma 4

Proof. From equation (A24), the demand function can be expressed as

$$q_{ijmt} = \nu_{jmt}^{\varepsilon} p_{ijmt}^{-\varepsilon} P_{ijt}^{\varepsilon-\sigma} P_{it}^{\sigma} Q_{it}, \tag{A31}$$

from which

$$\widehat{q}_{ijm} = \widehat{\nu}_{jm}^{\varepsilon}\widehat{p}_{ijm}^{-\varepsilon}\widehat{P}_{ij}^{\varepsilon-\sigma}\widehat{P}_i^{\sigma}\widehat{Q}_i \qquad \text{and} \qquad p_{ijc} = \left(\frac{1}{\widehat{q}_{ijc}}\widehat{P}_{ij}^{\varepsilon-\sigma}\widehat{P}_i^{\sigma}\widehat{Q}_i\right)^{\frac{1}{\varepsilon}}, \tag{A32}$$

where

$$\widehat{P}_{ij} = \frac{\left(\sum_{m\in M_{ij}} (\widehat{\nu}_{jm}\nu_{jm})^{\varepsilon}(\widehat{p}_{ijm}p_{ijm})^{1-\varepsilon}\right)^{\frac{1}{1-\varepsilon}}}{\left(\sum_{m\in M_{ij}} \nu_{jm}^{\varepsilon} p_{ijm}^{1-\varepsilon}\right)^{\frac{1}{1-\varepsilon}}} \tag{A33}$$

$$\widehat{P}_{i} = \frac{\left[\widehat{P}_{ii}^{\sigma} P_{iit}^{1-\sigma} + \sum_j \left(\sum_{m\in M_{ij}} (\widehat{\nu}_{jm}\nu_{jm})^{\varepsilon}(\widehat{p}_{ijm}p_{ijmt})^{1-\varepsilon}\right)^{\frac{1-\sigma}{1-\varepsilon}}\right]^{\frac{1}{1-\sigma}}}{\left[P_{iit}^{1-\sigma} + \sum_j \left(\sum_{m\in M_{ij}} \nu_{jmt}^{\varepsilon} p_{ijmt}^{1-\varepsilon}\right)^{\frac{1-\sigma}{1-\varepsilon}}\right]^{\frac{1}{1-\sigma}}} \tag{A34}$$

$$\widehat{Q}_{i} = \frac{\left[\widehat{Q}_{ii} Q_{iit}^{\frac{\sigma-1}{\sigma}} + \sum_j \left(\sum_{m\in M_{ij}} \widehat{\nu_{ijm}}\nu_{ijmt}(\widehat{q_{ijm}}q_{ijmt})^{\frac{\varepsilon-1}{\varepsilon}}\right)^{\frac{\varepsilon(\sigma-1)}{\sigma(\varepsilon-1)}}\right]^{\frac{\sigma}{\sigma-1}}}{\left[Q_{iit}^{\frac{\sigma-1}{\sigma}} + \sum_j \left(\sum_{m\in M_{ij}} \nu_{ijmt} q_{ijmt}^{\frac{\varepsilon-1}{\varepsilon}}\right)^{\frac{\varepsilon(\sigma-1)}{\sigma(\varepsilon-1)}}\right]^{\frac{\sigma}{\sigma-1}}} \tag{A35}$$

In addition, equation (A32) also allows us to express optimal demand for mode m' on route ij in terms mode m :

$$q_{ijm't} = q_{ijmt}\left(\frac{\nu_{jm't}}{\nu_{jmt}}\right)^{\varepsilon}\left(\frac{p_{ijmt}}{p_{ijm't}}\right)^{\varepsilon}, \tag{A36}$$

from which

$$\widehat{q_{ijm'}} = \widehat{q_{ijm}}\left(\frac{\widehat{\nu_{jm'}}}{\widehat{\nu}_{jm}}\right)^{\varepsilon}\left(\frac{\widehat{p_{ijm}}}{\widehat{p_{ijm'}}}\right)^{\varepsilon}. \tag{A37}$$

Turning to the second part of the Lemma, consider that a 1% increase in the containerized ocean freight rate causes a ζ_m% increase in the freight rate of mode m. In that case the change in the delivered price of the good delivered by m can be derived as following:

$$\widehat{p}_{ijm}(\widehat{p_{jc}}) = \left(\zeta_m\left(\alpha(\widehat{p_{ijc}}) - 1\right) + 1\right) p_{ijm} \text{ for } m \neq c \text{ given } \alpha(\widehat{p_{ijc}}) = \frac{\widehat{p_{jc}}p_{ijct} + p_{ijct}^{\text{FOB}}(1+\tau_{ijct})}{f_{ijct}} \tag{A38}$$

□

A.4.5 Proof of Lemma 5

Proof. For this exercise, we assume a representative vessel type for route ij which moves at speed s_{ijt}. Following Corbett et al. (2009), we use the following formula for its fuel cost per trip:

$$\text{Fuel cost per trip per vessel}(s_{ijt}) = \underbrace{\left[F^{\text{Main}}\left(\frac{s_{ijt}}{s_v^{\text{Des}}}\right)^3 + F^{\text{Aux}}\right]\frac{d_{ij}}{s_{ijt}}}_{=\text{Fuel consumption (ton)}} \times \underbrace{b}_{=\text{Bunker price (per ton)}},$$

where s_{ijt} and s_{ij}^{Des} are actual and design speeds, respectively; F^{Main} and F^{Aux} are main and auxiliary engine technological parameters respectively; d_{ij} is the distance per voyage; and b is the bunker cost per ton.

Adopting hat notation such that $\widehat{x} = x_T/x_t$, denote the change in the fuel cost per trip as a function of change in speed:

$$\widehat{\text{Fuel}}_{ij}(\widehat{s}_{ij}) = \widehat{b}\left[\frac{F^{\text{Main}}\left(\frac{\widehat{s}_{ij}s_{ijt}}{s_v^{\text{Des}}}\right)^3 + F^{\text{Aux}}}{F^{\text{Main}}\left(\frac{s_{ij}}{s_v^{\text{Des}}}\right)^3 + F^{\text{Aux}}}\right]\frac{1}{\widehat{s}_{ij}}$$

We assume that non-fuel expenses are proportional to total route time. Changes in trip time are inversely proportional to the change in round trips. If the number of round trips per year (e.g. the number voyages) at speed s_{ijt} is $n_{ijt} = \frac{A}{2(d_{ij}/(24s_{ijt})+port)} = \frac{A}{2(\text{Route time}_{ij})}$ and if we also allow for port congestion, then:

$$\widehat{n}_{ij}(\widehat{s}_{ij};\widehat{q}_{ijc}) = \widehat{s}_{ij}\left(\frac{d_{ij}+24s_{ijt}\overline{\text{port}}}{d_{ij}+24\widehat{s}_{ij}s_{ijt}\overline{\text{port}}(\widehat{q}_{ijc})^{\kappa}}\right) = \frac{1}{\widehat{\text{Route time}}(\widehat{s}_{ij};\widehat{q}_{ijc})} \tag{A39}$$

Note that in the long-run, changes in the number of round-trips is distinct from the change in route capacity $\widehat{q}_{ijc}$. Next. since changes in the number of round trips are inversely proportional to round-trip time, changes in our preference parameter ν can be written compactly by:

$$\widehat{\nu}^{LR} = \frac{\nu_{ij}^{LR}}{\nu_{ijt}} = \left(\frac{1}{\widehat{n}_{ij}(\widehat{s}_{ij};\widehat{q}_{ijc})}\right)^{-\beta_k} \tag{A40}$$

Assuming that $k_0 = \frac{1-\mu_{\text{Fuel}}}{\mu_{\text{Fuel}}}$ and that bunker fuel doesn't change, we can write the relative change to marginal cost as:

$$\begin{aligned}
\widehat{c}_{jc}(\widehat{s}_{ij};\widehat{q}_{ijc}) =& \frac{\widehat{\text{Fuel}}_{ij}\times\text{Fuel}_{ij} + \widehat{\text{Other}}_{ij}\times\text{Other}_{ij}}{\text{Fuel}_{ij}+\text{Other}_{ij}} \\
=& \frac{\widehat{\text{Fuel}}_{ij}\times\text{Fuel}_{ij} + \widehat{\text{Other}}_{ij}\times k_0\text{Fuel}_{ij}}{\text{Fuel}_{ij}(1+k_0)} \\
=& \frac{1}{k_0+1}\left(\widehat{\text{Fuel}}_{ij}\times\widehat{\text{Other}}_{ij}k_0\right) \\
=& \frac{1}{k_0+1}\left(\left[\frac{F^{\text{Main}}\left(\frac{\widehat{s}_{ij}s_{ij}}{s_v^{\text{Des}}}\right)^3 + F^{\text{Aux}}}{F^{\text{Main}}\left(\frac{s_{ij}}{s_v^{\text{Des}}}\right)^3 + F^{\text{Aux}}}\right]\frac{1}{\widehat{s}_{ij}} + \frac{k_0}{\widehat{n}_{ij}(\widehat{s}_{ij};\widehat{q}_{ijc})}\right) \\
=& \mu_{\text{Fuel}}\left(\left[\frac{F^{\text{Main}}\left(\frac{\widehat{s}_{ij}s_{ij}}{s_v^{\text{Des}}}\right)^3 + F^{\text{Aux}}}{F^{\text{Main}}\left(\frac{s_{ij}}{s_v^{\text{Des}}}\right)^3 + F^{\text{Aux}}}\right]\frac{1}{\widehat{s}_{ij}}\right) + \frac{(1-\mu_{\text{Fuel}})}{\widehat{n}_{ij}(\widehat{s}_{ij};\widehat{q}_{ijc})}
\end{aligned} \tag{A41}$$

□

A.5 Estimating the Containerized Shipping Price elasticity of Air-Shipping Price

Given the substantial excess capacity previously identified in the air-shipping industry, it's unclear if an expected rise in ocean freight rates would correspondingly boost air freight rates. To further investigate, we analyze US imports data from 2013 to 2019 A.5. The data, organized on a monthly-(HS6 product)-(customs

district)-(exporting country) basis, is used to estimate the relationship between these two freight rates. Our simple pass-through model has ad-valorem iceberg associated with the air-transported imports $\overline{\phi}_{ijkt}$ (defined as the ratio of the factory price and air freight rate over factory price) regressed on the corresponding iceberg cost of vessel imports (ϕ_{ijkt}):

$$\ln(\overline{\phi}_{ijkt}) = \beta_1 \ln(\phi_{ijkt}) + \beta_2 \ln(bunker_t) + \theta_{ijk} + \mu_{ijkt}$$

where, as controls, we also include the average monthly high sulfur bunker fuel cost (USD/tonne) across 400 ports from Clarksons SIN, $bunker_t$ and (HS6 product)-(customs district)-(exporting country) fixed effects.

The results are presented in Table A9. The "pass through" estimate of β_1 is the primary object of interest. We find it to be 0.021, an economically insignificant figure. For instance, a 5% increase in the average ad-valorem vessel rate in 2019 (from 1.048 to 1.10) would result in a mere 0.011% rise in the average ad-valorem air rate (from 1.123 to 1.1242). In other words, doubling the vessel freight rate would only lead to a 1% increase in air freight rates. In our analysis, we also include as controls the average monthly high sulfur bunker fuel cost (USD/tonne) across 400 ports from Clarksons SIN, denoted as $bunker_t$, along with (HS6 product)-(customs district)-(exporting country) fixed effects. Our primary focus is the "pass-through" estimate of β_1. We find it to be 0.021, an economically insignificant figure. To illustrate, a 5% rise in the average ad-valorem vessel rate in 2019 (from 1.048 to 1.10) would trigger just a 0.011% increase in the average ad-valorem air rate (from 1.123 to 1.1242). Simply put, if the vessel freight rate were to double, it would lead to a 1% increase in air freight rates.

Table A9: Simple Pass Through Model

	(1)
$\ln(\phi_{ijkt})$	0.021^{***}
	(0.001)
$\ln(bunker_t)$	0.007^{***}
	(0.000)
Num. obs.	$18,849,010$
FE: District i × Country j × HS6 k	$620,230$
R^2	0.437
Adj. R^2	0.418

Notes: $^{***}p < 0.01$; $^{**}p < 0.05$; $^{*}p < 0.1$

A.6 Deriving Long-run Changes in Ocean and Air Transportation

This section presents an ex-ante derivation of the long-run changes resulting from the implementation of IMO2023. in air- Our approach utilizes a theoretical model, shipping cost structure, and naval engineering formulas. In accordance with the derivation presented in equation (20), we can calculate changes in prices for each transportation mode.

For each custom district i and a vector of slowdown speeds ($\widehat{s}_{ij}$), pick a value of $\widehat{Q}_i$.

Iteration Cycle I: For each route, find $\widehat{q}_{ijc}$:

1. Initialize a guess on $\widehat{q}_{ijc} = 1$.
2. Using change in route volume with equation (A39) to calculate changes in round trips;
3. Using equation (18) to calculate changes in trip marginal cost and apply the obtained changes to calculate freight rates using equation (19);
4. Use equation (20) to calculate changes in all delivered prices;
5. Using equation (A35) to compute changes in the aggregated price and quantity indices;
6. Using equation (A42), verify that initial guess $\widehat{q}_{ijc}$ is consistent. In practice, we employ a fixed point algorithm to solve for such a $\widehat{q}_{ijc}$.

$$\widehat{q}_{ijc} = \widehat{v}_{jm}^{\varepsilon\frac{\sigma-1}{\varepsilon-1}} \widehat{p}_{ijm}^{-\varepsilon} \widehat{P}_{ij}^{\varepsilon-\sigma} \widehat{P}_i^{\sigma} \widehat{Q}_i(\widehat{q}_{ijm}; \widehat{Q}_i) \tag{A42}$$

given that:

$$\widehat{Q}_i(\widehat{q}_{ijm}; \widehat{Q}_i) = \frac{\left[(\widehat{Q}_i Q_i)^{\frac{\sigma-1}{\sigma}} + \sum_j \left(\sum_{m \in M_{ij}} \widehat{v}_{jm} v_{jm} (\widehat{q}_{ijm} q_{ijm})^{\frac{\varepsilon-1}{\varepsilon}} \right)^{\frac{\varepsilon(\sigma-1)}{\sigma(\varepsilon-1)}} \right]^{\frac{\sigma}{\sigma-1}}}{\left[Q_i^{\frac{\sigma-1}{\sigma}} + \sum_j \left(\sum_{m \in M_{ij}} v_{jm} q_{ijm}^{\frac{\varepsilon-1}{\varepsilon}} \right)^{\frac{\varepsilon(\sigma-1)}{\sigma(\varepsilon-1)}} \right]^{\frac{\sigma}{\sigma-1}}} \tag{A43}$$

Iteration Cycle II: Once we have found $\widehat{q}_{ijc}$ that is consistent with itself and is based on $\widehat{Q}_i$, check that new total expenditure satisfies the budget constraint within some error tolerance. If not, we choose a different value of $\widehat{Q}_i$ and repeat the above steps until error tolerance is satisfied.

A.7 Data Analysis of Shipping Speed and Route Stability

When analyzing IMO2023, we assume that routes are stable and will not be affected by the reform. In this section, we provide support for this assumption through the distribution of two types of route stability measures. The first measure is the **route-specific coefficient of variation of ports** which is calculated as the ratio of the standard deviation of number of ports to the average number of ports. The higher the measure, the more (relatively) disperse the number of ports are on a given route.

The second route stability measure, **"Port Share,"** is defined as the average number of ports used by a given route in a given month, normalized by the total number of ports that the route ever uses. The formula to calculate it is:

$$\text{Port Share}_{ijt} = \frac{1}{|T_{ij}||n_{ij}|} \sum_{t_{ij} \in T_{ij}} n_{ij}(t_{ij})$$

Here, T_{ij} is the number of time periods that route ij appears, n_i is the list of all ports ever used by route ij, and $n_{ij}(t_{ij})$ is the number of ports used by rotation ij for month t. A score of zero (one) means no (perfect) port overlap for a given route.

Table A10 lists our stability results. The average port share of roughly 60% suggests that on average, each route uses 60% of its total ports in a given month. This indicates that, at least on a short-term basis, the routes are relatively stable and not subject to significant changes. The coefficient of variation, which measures the dispersion of the number of ports used by a route, is close to 20%, indicating that there is some variability in the number of ports used by different routes, but overall the routes remain relatively stable.

Table A10: Route Stability Measures

Stat	Port Coefficient of Variation	Port Share
Min.	0.0%	15.4%
1st Qu.	6.9	43.5
(I)	16.5	54.3
Mean	19.4	59.5
3rd Qu.	28.7	73.6
Max.	105.3	100.0

A.8 Land Transport Mode Carbon Efficiencies

TransBorder data features different land based transport modes that facilitate trade with the United States. Each mode with its corresponding carbon efficiency rating, sourced from the Congressional Budget Office (CBO), is listed in the table below:

Table A11: Carbon Emission Factors

Code	Mode	CO_2 lbs per ton-mile	CO_2 grams per ton-mile
4	Mail (U.S. Postal Service)	0.40	181.4
5	Truck	0.40	181.4
6	Rail	0.05	22.68
7	Pipeline	0.13	58.97

For each import route between a U.S. Custom District i and Mexico/Canada, we use the total import volume (by weight) as weights in computing an average of land transport based import routes CO_2 emission factors.

A.9 Geography of U.S. Custom Districts

Each U.S. Custom District is made up of different ports; these ports are found in the U.S. Census Bureau's International Trade Schedule D - District and Port Codes and Descriptions. To the best of our knowledge, there are no publically available GIS shapefiles or other sources of spatial data that provide the geographic boundaries of each U.S. Custom District. For the purposes of our analysis, we treat U.S. Custom Districts as a population weighted centroid. To estimate this centorid, we geocode each port that belongs to U.S. Custom District i. Armed with a port's coordinates, we then use the Global Rural-Urban Mapping Project, Version 1 (GRUMPv1): Settlement Points to find the closet human settlement (e.g., city, town, incoporated area, etc.) and use that settlement's population as an average-weight when computing Custom District i's average longitude/latitude. Figure A6 displays the results of this data-building task.

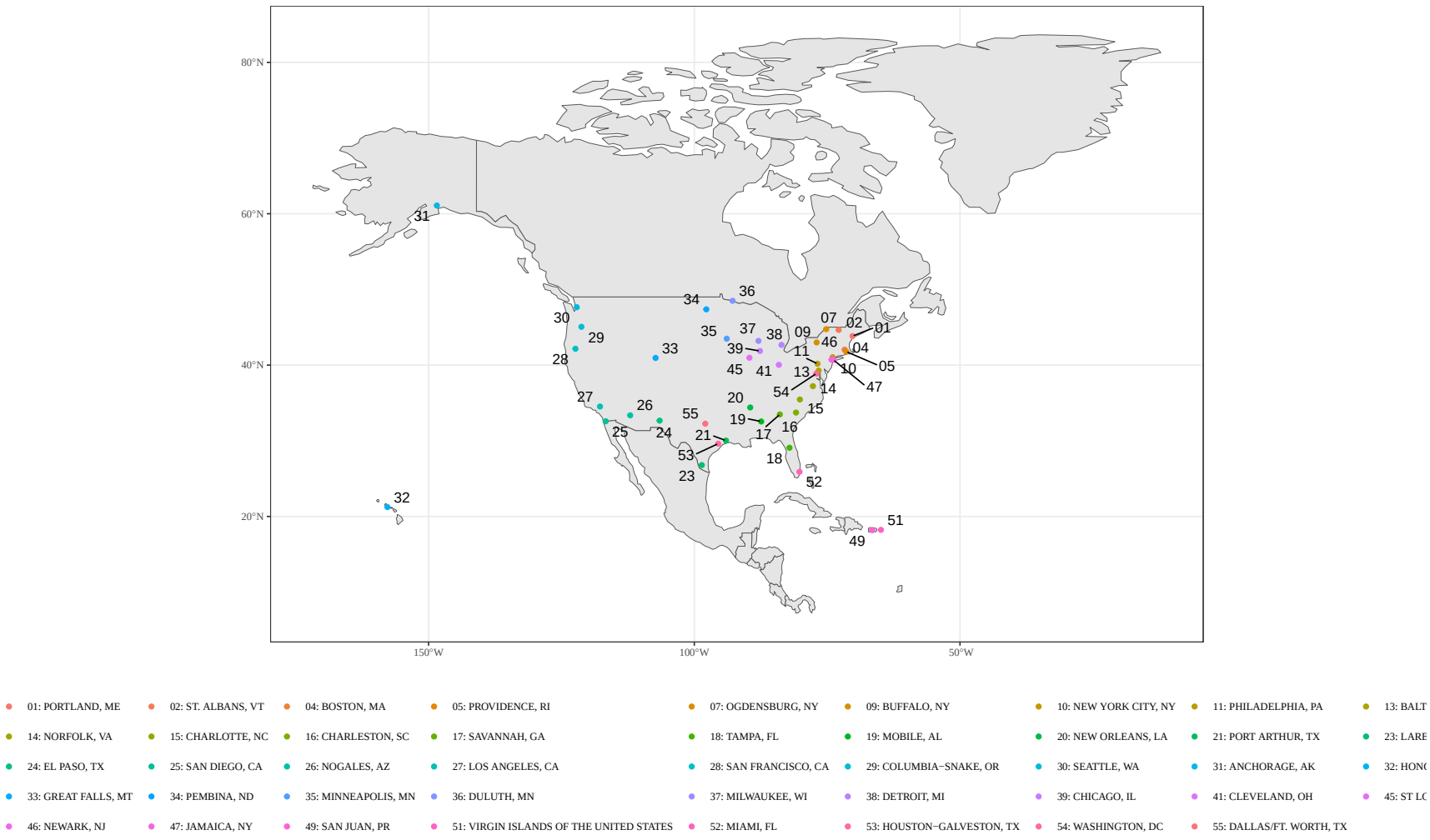


Figure A6: U.S. Custom Districts (Population Weighted Centroids)

A.10 Air Transport Share of Manufacturing Imports by Country

Table A12: Shares of manufacturing imports transported by air

Importer	Air share by weight	Cumul. share by weight	Air share by value	Cumul. share by value
Algeria	0.03	0.10	0.24	0.02
Germany	0.01	0.03	0.27	0.05
Türkiye	0.00	0.00	0.29	0.06
Spain	0.01	0.02	0.29	0.07
Australia	0.02	0.06	0.30	0.08
Brazil	0.01	0.01	0.33	0.09
France	0.04	0.14	0.41	0.13
Czechia	0.05	0.21	0.43	0.14
Russia	0.07	0.37	0.43	0.15
Italy	0.03	0.07	0.45	0.17
Poland	0.04	0.16	0.46	0.19
Saudi Arabia	0.04	0.11	0.51	0.21
Indonesia	0.05	0.22	0.52	0.22
Romania	0.10	0.65	0.52	0.22
Belgium	0.04	0.12	0.53	0.24
United States	0.09	0.62	0.54	0.44
Netherlands	0.04	0.18	0.57	0.47
Philippines	0.06	0.25	0.59	0.48
United Kingdom	0.02	0.04	0.59	0.51
Viet Nam	0.02	0.05	0.60	0.53
Thailand	0.08	0.40	0.62	0.54
Korea, Republic of	0.05	0.20	0.63	0.58
Ireland	0.05	0.23	0.64	0.59
Austria	0.09	0.64	0.65	0.60
Japan	0.14	0.82	0.69	0.65
India	0.13	0.74	0.72	0.68
Switzerland	0.02	0.03	0.73	0.70
China	0.06	0.34	0.73	0.85
United Arab Emirates	0.09	0.63	0.76	0.88
Singapore	0.17	0.86	0.83	0.92
China, Hong Kong	0.33	0.95	0.83	0.99
Malaysia	0.56	0.98	0.90	1.00

Notes: Shares are calculated from UNCTAD Global Transport Dataset (Hoffmeister et al., 2022). The following countries are excluded because their share in total value of manufacturing goods shipped by air in 2021 is less that 0.5% Afghanistan, Albania, Andorra, Angola, Argentina, Armenia, Azerbaijan, Bahrain, Belarus, Belize, Benin, Bolivia (Plurinational State of), Bosnia and Herzegovina, Botswana, Brunei Darussalam, Bulgaria, Burkina Faso, Burundi, Cabo Verde, Cambodia, Cameroon, Central African Republic, Chile, China, Macao SAR, Colombia, Congo, Dem. Rep. of the, Croatia, Cyprus, Côte d'Ivoire, Denmark, Dominican Republic, Ecuador, Egypt, El Salvador, Estonia, Eswatini, Ethiopia, Finland, Georgia, Ghana, Greece, Guatemala, Guinea, Guyana, Honduras, Hungary, Iceland, Iran (Islamic Republic of), Israel, Jamaica, Jordan, Kazakhstan, Kenya, Kiribati, Kyrgyzstan, Lao People's Dem. Rep., Latvia, Lebanon, Libya, Lithuania, Luxembourg, Madagascar, Malawi, Maldives, Mali, Malta, Mauritania, Moldova, Republic of, Mongolia, Montenegro, Montserrat, Morocco, Mozambique, Myanmar, Namibia, Nepal, New Zealand, Nicaragua, Niger, Nigeria, North Macedonia, Norway, Oman, Pakistan, Palau, Panama, Paraguay, Peru, Portugal, Qatar, Rwanda, Saint Vincent and the Grenadines, Samoa, Sao Tome and Principe, Senegal, Serbia, Sierra Leone, Slovakia, Slovenia, Sri Lanka, State of Palestine, Sudan, Sweden, Tajikistan, Tanzania, United Republic of, Timor-Leste, Togo, Tunisia, Uganda, Ukraine, Uruguay, Uzbekistan, Yemen, Zambia, Zimbabwe